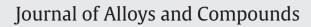
Contents lists available at ScienceDirect







journal homepage: www.elsevier.com/locate/jallcom

# Subject Index of Volume 506

A356 alloy	Amorphous materials
structural, mechanical and tribological properties of A356 aluminium alloy	microstructure and thermal stability of amorphous SiBCNAl powders
reinforced with Al <sub>2</sub> O <sub>3</sub> , SiC and SiC + graphite particles 631	fabricated by mechanical alloying 88
AA7000 aluminum alloy	glass-crystal transformations in $Se_{80-x}Te_{20}Ag_x$ (x = 0, 3, 5, 7 and 9) glasses
structure and consolidation of rapidly solidified Meso 10 alloy flakes 179	956
Ab initio calculations	Amorphous semiconductors
prediction study of the axial compressibility, anisotropy and dynamic properties for single crystal Ti <sub>2</sub> GeC 22	composition dependent of dielectric properties in $\text{Se}_{100-x}\text{Sn}_x$ glassy alloys 710 Annealing
Absorption spectra spectroscopic and crystal field studies of LiAlO <sub>2</sub> :Mn <sup>2+</sup> single crystals 4	changes in short-range order of Zr <sub>55</sub> Cu <sub>30</sub> Al <sub>10</sub> Ni <sub>5</sub> and Zr <sub>55</sub> Cu <sub>20</sub> Al <sub>10</sub> Ni <sub>10</sub> Ti <sub>5</sub> BMGs upon annealing 85
Additivity	Anode
quantitative analysis of crystalline and remaining glass phases in CaO-B <sub>2</sub> O <sub>3</sub> - SiO <sub>2</sub> ternary system glass ceramics 757	influence of Li addition on charge/discharge behavior of spinel lithium titanate 231
AFM	synthesis and electrochemical properties of pure phase Zn <sub>2</sub> SnO <sub>4</sub> and
electrochemical corrosion behavior in NaCl medium of zinc-nickel alloys electrodeposited under applied magnetic field 575	composite Zn <sub>2</sub> SnO <sub>4</sub> /C 683 Antiferroelectric
Age-hardening	the phase evolution with temperature in 0.94PbZrO <sub>3</sub> -0.06Pb(Mg <sub>1/2</sub> W <sub>1/2</sub> )O <sub>3</sub>
phase transformation and age-hardening of hexagonal $\alpha'$ martensite in Ti–	antiferroelectric ceramic 313
12 mass%V-2 mass%Al alloys studied by transmission electron	Antiferromagnetism
microscopy 607	antiferromagnetism of $LnRhO_3$ ( $Ln = rare earth$ ) 27
AgInS <sub>2</sub>	ARB
study of the <i>I–V</i> characteristics of SnO <sub>2</sub> :F/AgInS <sub>2</sub> (p)/AI Schottky diodes 492	high-strength and high-conductive Cu/Ag multilayer produced by ARB 172
Agricultural pollutants	Arc-discharge
immobilized titania nanophotocatalysis: Degradation, modeling and toxicity	enhanced absorption bandwidth in carbon-coated supermalloy FeNiMo
reduction of agricultural pollutants 155	nanocapsules for a thin absorb thickness 826
Al doping	Atomic force microscopy
effect of Al doping on the visible photoluminescence of ZnO nanofibers 772	study of obliquely deposited thin cobalt films 526
Alloy and microstructure	AZ31
phase transformation of metastable cubic $\gamma$ -phase in U–Mo alloys 253	microstructural evolution during the annealing of an extruded AZ31
Al-Mg alloy	magnesium alloy 364
microstructure evolution and precipitation of Al-12Mg alloy solidified under	AZ31/Al <sub>2</sub> O <sub>3</sub> composites
high pressure L12	mechanical property retention in remelted microparticle to nanoparticle
Al-Ni-RE ternary alloys	AZ31/Al <sub>2</sub> O <sub>3</sub> composites 600
calculation of glass forming ranges in Al-Ni-RE (Ce, La, Y) ternary alloys and	
their sub-binaries based on Miedema's model 377	BaCoO <sub>3</sub>
Ammonia	pervoskite-type $BaCo_{0,7}Fe_{0,2}Ta_{0,1}O_{3-\delta}$ cathode for proton conducting IT-SOFC
structural and thermal gas desorption properties of metal aluminum amides	L8
297	Ball grid array solder joints
Amorphisation	the influence of addition of Al nano-particles on the microstructure and
glass-crystal transformations in $Se_{80-x}Te_{20}Ag_x$ (x = 0, 3, 5, 7 and 9) glasses 956	shear strength of eutectic Sn–Ag–Cu solder on Au/Ni metallized Cu pads 216
Amorphization	Ball milling
amorphization of equimolar alloys with HCP elements during mechanical alloying 210	the effects of nanometric nickel (n-Ni) catalyst on the dehydrogenation and rehydrogenation behavior of ball milled lithium alanate (LiAlH <sub>4</sub> ) 928
Amorphous	Barium cerate
calculation of glass forming ranges in Al–Ni–RE (Ce, La, Y) ternary alloys and their sub-binaries based on Miedema's model 377	stability and electrical property of Ba <sub>1-x</sub> Sr <sub>x</sub> Ce <sub>0.8</sub> Y <sub>0.2</sub> O <sub>3-δ</sub> high temperature proton conductor 263
Amorphous alloys	Barrier height
crystallization kinetics of Mg <sub>61</sub> Cu <sub>28</sub> Gd <sub>11</sub> and (Mg <sub>61</sub> Cu <sub>28</sub> Gd <sub>11</sub> ) <sub>99.5</sub> Sb <sub>0.5</sub> bulk metallic glasses 302	investigations on the nonidealities in Pd/n-GaN Schottky diodes grown by MOCVD 615

Barrier inhomogeneities

- measurement and modelling of the characteristic parameters for silver Schottky contacts on layered *p*-GaSe compound in a wide temperature range 51
- analysis of barrier height inhomogeneity in Au/n-GaAs Schottky barrier diodes by Tung model 418

Barrier inhomogeneity

- analysis of the electrical characteristics of *Zn/ZnSe/n-Si/Au–Sb* structure fabricated using SILAR method as a function of temperature 388
- BGaAs
  - growth temperature effects on boron incorporation and optical properties of BGaAs/GaAs grown by MOCVD 10

BiFeO<sub>3</sub>-based solid solutions

- preparation and properties of (1 *x*)BiFeO<sub>3</sub>–*x*BaTiO<sub>3</sub> multiferroic ceramics 862
- Bimetallic system
  - preparation, characterization and utilization of (Ni:Cu) bimetallic system loaded on zeolites 923

## Binary

- synthesis of CIGS powders: Transition from binary to quaternary crystalline structure 969
- Bi-Pb-Cu glass

ferroelectricity in the glassy material of the composition  $Bi_2O_3$ -Pb $_3O_4$ -CuO-K<sub>2</sub>O 141

Bitter pattern technique

study of obliquely deposited thin cobalt films 526

- Bulk metallic glasses
  - changes in short-range order of  $Zr_{55}Cu_{30}Al_{10}Ni_5$  and  $Zr_{55}Cu_{20}Al_{10}Ni_{10}Ti_5$  BMGs upon annealing  $\,85$

## CaCu<sub>3</sub>Ti<sub>4</sub>O<sub>12</sub>

- effect of vanadium doping on the dielectric and nonlinear current–voltage characteristics of CaCu<sub>3</sub>Ti<sub>4</sub>O<sub>12</sub> ceramic 853 Cadmium telluride
  - comparative study of electrical properties of Cd and Te-enriched CdTe thin films at cryogenic temperature 661
- Carbon fiber

magnetic properties and microwave absorption properties of carbon fibers coated by Fe<sub>3</sub>O<sub>4</sub> nanoparticles 93

- Catalytic activity
  - synthesis, characterization and physicochemical properties of nanosized Zn/Mn oxides system 541

## Cathode

- pervoskite-type  $BaCo_{0.7}Fe_{0.2}Ta_{0.1}O_{3-\delta}$  cathode for proton conducting IT-SOFC L8
- synthesis of  $LiNi_{0.65}Co_{0.25}Mn_{0.1}O_2$  as cathode material for lithium-ion batteries by rheological phase method 888

Cathode material

a novel process for producing synthetic rutile and LiFePO<sub>4</sub> cathode material from ilmenite 271

## CBD

phase evolution and PEC performance of  $Zn_xCd_{(1-x)}S$  nanocrystalline thin films deposited by CBD 120

CCTO ceramic

structure and electrical response of CaCu<sub>3</sub>Ti<sub>4</sub>O<sub>12</sub> ceramics: Effect of heat treatments at the high vacuum L1

#### Cd0

the importance of the methanol content in the precursor solution, on the physical properties of cadmium oxide thin films prepared by the sol-gel method 554

Ceramic nuclear waste

- calorimetric investigations on cubic  ${\rm BaTiO_3}$  and  ${\rm Ba}_{0.9}{\rm Nd}_{0.1}{\rm TiO_3}$  systems 565 Ceramic–matrix nanocomposites
- compressibility and sinterability of Al<sub>2</sub>O<sub>3</sub>–YAG nanocomposite powder synthesized by an aqueous sol–gel method 640

#### Ceramics

- phase-transition behavior and piezoelectric properties of lead-free  $(Ba_{0.95}Ca_{0.05})(Ti_{1-x}Zr_x)O_3$  ceramics 131
- enhanced thermoelectric properties of Nb-doped SrTiO<sub>3</sub> polycrystalline ceramic by titanate nanotube addition 293 size effect on the magnetic property of CoAl<sub>2</sub>O<sub>4</sub> nanopowders prepared by reverse micelle processing 395 synthesis and characterization of nano-crystalline  $Ce_{1-x}Gd_xO_{2-x/2}$  (x = 0-0.30) solid solutions 739 quantitative analysis of crystalline and remaining glass phases in CaO-B2O3-SiO<sub>2</sub> ternary system glass ceramics 757 multiferroic properties of BiFeO<sub>3</sub> doped Bi(MgTi)O<sub>3</sub>-PbTiO<sub>3</sub> ceramic system 815 Chalcogenide glasses composition dependent of dielectric properties in  $Se_{100-x}Sn_x$  glassy alloys Chalcopyrite study of the I-V characteristics of SnO<sub>2</sub>:F/AgInS<sub>2</sub> (p)/Al Schottky diodes 492 Characterizations synthesis and characterization of AgI thin films at low temperature 268 size effect on the magnetic property of  $CoAl_2O_4$  nanopowders prepared by reverse micelle processing 395 Chelating agent development of cobalt ferrite powder preparation employing the sol-gel technique and its structural characterization 400 Chemical bath deposition n-Type polycrystalline (CdZn)Se photoelectrode synthesis and its photoelectrochemical characterizations 673 Chemical method synthesis and characterization of AgI thin films at low temperature 268 Chemical synthesis tuning visible emission by choosing excitation wavelength in Mg-doped ZnO/silica composites 1 temperature dependence of morphology, structural and optical properties of ZnS nanostructures synthesized by wet chemical route 249 growth of novel ZnO nanostructures by soft chemical routes 351 size effect on the magnetic property of CoAl<sub>2</sub>O<sub>4</sub> nanopowders prepared by reverse micelle processing 395 structural study and properties of a new iron phosphate  $Rb_9Fe_7(PO_4)_{10}$  569 synthesis and characterization of nano-crystalline  $Ce_{1-x}Gd_xO_{2-x/2}$  (x = 0-0.30) solid solutions 739 temperature dependent structural, luminescent and XPS studies of CdO:Ga thin films deposited by spray pyrolysis 794 one-pot synthesis of Zn<sub>v</sub>Cd<sub>1-v</sub>S nanocrystals with tunable optical properties from molecular precursors 804 structural, morphological and optical properties of nanocrystalline cadmium selenide thin films 849 effects of annealing on cadmium selenide nanocrystalline thin films prepared by chemical bath deposition 892 effects of types of drying control chemical additives on the morphologies and electrochemical properties of Li<sub>4</sub>Ti<sub>5</sub>O<sub>12</sub> anode powders prepared by spray pyrolysis 913 synthesis of zinc oxide nanoparticles elaborated by microemulsion method 944 CIGS synthesis of CIGS powders: Transition from binary to quaternary crystalline structure 969 Coating materials laser remelting of plasma-sprayed conventional and nanostructured Al2O3-13 wt.%TiO<sub>2</sub> coatings on titanium alloy 356 the effects of calcination temperature on the electrochemical performance of LiMnPO<sub>4</sub> prepared by ultrasonic spray pyrolysis 372 temperature dependent structural, luminescent and XPS studies of CdO:Ga thin films deposited by spray pyrolysis 794 Coatings

synthesis, characterization and properties of  $Ln(Ti_{0.8}Sn_{0.2})TaO_6$  (Ln = Nd, Sm)

microwave ceramics 243

- microstructural characteristics and degradation mechanism of the NiCrAlY/CrN/DSM11 system during thermal exposure at 1100 °C 77
- comparative study of electrical properties of Cd and Te-enriched CdTe thin films at cryogenic temperature 661

Cobalt ferrite nanoparticles

development of cobalt ferrite powder preparation employing the sol-gel technique and its structural characterization 400

Cobaltite

epitaxial growth of La<sub>0.7</sub>Sr<sub>0.3</sub>CoO<sub>3</sub> thin films on SrTiO<sub>3</sub> substrates by metalorganic deposition 483

Colloidal method

- ${\rm RuO_2-SnO_2}$  nanocomposite electrodes for methanol electrooxidation 57 Color center
- light-induced coloration and transformation process in  $\mathrm{YAlO}_3\,\mathrm{crystal}~500$  Compaction
  - compressibility and sinterability of Al<sub>2</sub>O<sub>3</sub>-YAG nanocomposite powder synthesized by an aqueous sol-gel method 640
- Complex permeability
  - a new microwave absorber based on antimony-doped tin oxide and ferrite composite with excellent electromagnetic match 347
- Complex permittivity
  - a new microwave absorber based on antimony-doped tin oxide and ferrite composite with excellent electromagnetic match 347

Compocasting

- structural, mechanical and tribological properties of A356 aluminium alloy reinforced with Al<sub>2</sub>O<sub>3</sub>, SiC and SiC + graphite particles 631 Composite coatings
- pulse co-electrodeposition and characterization of NiW-WC composite coatings 151

Composite foams

- deformation and energy absorption characteristic of Al<sub>2</sub>O<sub>3f</sub>/Zn–Al composite foams during compression 620
- Composite materials
- a new microwave absorber based on antimony-doped tin oxide and ferrite composite with excellent electromagnetic match 347

Compressive behavior

deformation and energy absorption characteristic of Al<sub>2</sub>O<sub>3f</sub>/Zn–Al composite foams during compression 620

Computer simulations

metal halide doped metal borohydrides for hydrogen storage: The case of  $Ca(BH_4)_2$ - $CaX_2$  (X = F, Cl) mixture 721

Conductivity

- high-strength and high-conductive Cu/Ag multilayer produced by ARB 172 preparation and characterization of Li<sub>5</sub>ReSi<sub>4</sub>O<sub>12</sub> (Re = Nd, Gd) solid electrolyte 811
- Converse magnetoelectric effect
  - multiferroic properties and converse magnetoelectric effect in Bi<sub>1-x</sub>Ca<sub>x</sub>FeO<sub>3</sub> ceramics 537
- Co-precipitation
  - luminescence and absorbance of highly crystalline CaMoO<sub>4</sub>, SrMoO<sub>4</sub>, CaWO<sub>4</sub> and SrWO<sub>4</sub> nanoparticles synthesized by co-precipitation method at room temperature 475

Core/shell microstructure

- catalyst-free combined synthesis of Zn/ZnO core/shell hollow microspheres and metallic Zn microparticles by thermal evaporation and condensation route 666
- Corrosion
  - controls of chromium and third element contents in nickel-base alloys for corrosion resistant alloys in hot HNO<sub>3</sub>–HF mixtures 194

electrochemical corrosion behavior in NaCl medium of zinc–nickel alloys electrodeposited under applied magnetic field 575

- Cr content
- controls of chromium and third element contents in nickel-base alloys for corrosion resistant alloys in hot HNO<sub>3</sub>–HF mixtures 194

Cr substitution

synthesis characterization and magnetic properties of Cr-substituted NiCuZn nanocrystalline ferrite 205

Cr<sub>2</sub>AlC

- synthesis and mechanical properties of nano-layered composite 734 Creep
- size dependence of creep behavior in nanoscale Cu/Co multilayer thin films  $\,$  434 Crosslinker  $\,$ 
  - development of cobalt ferrite powder preparation employing the sol-gel technique and its structural characterization 400

- $Cr_{1-x}Ti_xSb_2$ 
  - the effect of Ti substitution for Cr on transport and thermoelectric properties of CrSb<sub>2</sub> at low temperatures 917

## Crystal field

spectroscopic and crystal field studies of  ${\rm LiAlO}_2{\rm :}{\rm Mn}^{2+}$  single crystals 4 Crystal growth

- temperature-dependent study of the band-edge excitonic transitions of Cu<sub>2</sub>ZnSiS<sub>4</sub> single crystals by polarization-dependent piezoreflectance 46 measurement and modelling of the characteristic parameters for silver
- Schottky contacts on layered *p*-GaSe compound in a wide temperature range 51
- effect of rare-earth dopants on the growth and structural, optical, electrical and mechanical properties of L-arginine phosphate single crystals 784
- the magneto-dielectric properties of compounds and alloys in the systems of TlInS<sub>2</sub>-TIFeS<sub>2</sub>, TlInS<sub>2</sub>-TIFeSe<sub>2</sub> 800

Crystal structure

effects of Fe substitution on structural and magnetic properties of the  $Nd_2Co_{7-x}Fe_x$  compounds 766

Crystalline field

- a facile one-pot hydrothermal method to prepare europium-doped titania hollow phosphors and their sensitized luminescence properties 728
- Crystallization kinetics
  - crystallization kinetics of  $Mg_{61}Cu_{28}Gd_{11}$  and  $(Mg_{61}Cu_{28}Gd_{11})_{99.5}Sb_{0.5}$  bulk metallic glasses 302
- Cu/Co multilayers
  - size dependence of creep behavior in nanoscale Cu/Co multilayer thin films 434

Cu-Ag

- high-strength and high-conductive Cu/Ag multilayer produced by ARB 172 Cubic barium titanate
- calorimetric investigations on cubic BaTiO<sub>3</sub> and Ba<sub>0.9</sub>Nd<sub>0.1</sub>TiO<sub>3</sub> systems 565 Cubic ZrO<sub>2</sub> phase
- preparation of partially stabilized zirconia from fused zirconia using roasting L5

Cubic-zirconia

- intrinsic vacancies in cubic-zirconia bulk and surface 898
- CuIn<sub>x</sub>Ga<sub>1-x</sub>Se<sub>2</sub>
- synthesis of CIGS powders: Transition from binary to quaternary crystalline structure 969

## CuO addition

- dielectric and piezoelectric characteristics of the non-stoichiometric (Na,K)NbO<sub>3</sub> ceramics doped with CuO 872
- Curie temperature
  - ferroelectricity in the glassy material of the composition Bi<sub>2</sub>O<sub>3</sub>-Pb<sub>3</sub>O<sub>4</sub>-CuO-K<sub>2</sub>O 141

## Damping capacities

effect of extrusion temperature on microstructures and damping capacities of Grp/AZ91 composite 688

## Dc conductivity

- ferroelectricity in the glassy material of the composition Bi<sub>2</sub>O<sub>3</sub>-Pb<sub>3</sub>O<sub>4</sub>-CuO-K<sub>2</sub>O 141 DDX
  - growth temperature effects on boron incorporation and optical properties of BGaAs/GaAs grown by MOCVD 10

## Decay time

time-resolved photoluminescence study of stabilised iron-porous silicon nanocomposites 496

## Defects

investigations on the nonidealities in Pd/n-GaN Schottky diodes grown by MOCVD 615

Degradation

immobilized titania nanophotocatalysis: Degradation, modeling and toxicity reduction of agricultural pollutants 155

## Density

phase transformation of metastable cubic  $\gamma$ -phase in U–Mo alloys 253 Density functional theory

mechanochemically driven nonequilibrium processes in MNH<sub>2</sub>-CaH<sub>2</sub> systems (M = Li or Na) 224

978

Elastic constants

phases in Mg-Sc-Zn alloy 412

Desorption temperature and kinetics

the effects of nanometric nickel (n-Ni) catalyst on the dehydrogenation and rehydrogenation behavior of ball milled lithium alanate (LiAlH<sub>4</sub>) 928 Dielectric constant

- study of electrical properties of nickel doped SnO<sub>2</sub> ceramic nanoparticles 237
- substituting La<sup>3+</sup> with Sr<sup>2+</sup> to improve microwave dielectric properties of La(Mg<sub>0.5</sub>Sn<sub>0.5</sub>)O<sub>3</sub> ceramics 441
- Dielectric properties
  - anisotropic properties and crystal structure of ferroelectric  $\mathrm{Na}_{0.5}\mathrm{Bi}_{4.5}\mathrm{Ti}_4\mathrm{O}_{15}$  70
  - crystal structure and properties of K<sub>0.5</sub>Na<sub>0.5</sub>NbO<sub>3</sub>-Bi<sub>0.5</sub>Na<sub>0.5</sub>TiO<sub>3</sub>-LiSbO<sub>3</sub> leadfree piezoelectric ceramics 407
  - composition dependent of dielectric properties in  ${\rm Se}_{100-x}{\rm Sn}_x$  glassy alloys 710
  - the magneto-dielectric properties of compounds and alloys in the systems of TlInS<sub>2</sub>-TlFeS<sub>2</sub>, TlInS<sub>2</sub>-TlFeSe<sub>2</sub> 800
  - effect of vanadium doping on the dielectric and nonlinear current-voltage characteristics of CaCu<sub>3</sub>Ti<sub>4</sub>O<sub>12</sub> ceramic 853

Dielectric spectroscopy

structure and electrical response of CaCu<sub>3</sub>Ti<sub>4</sub>O<sub>12</sub> ceramics: Effect of heat treatments at the high vacuum L1

Dielectric study

effect of rare-earth dopants on the growth and structural, optical, electrical and mechanical properties of L-arginine phosphate single crystals 784 Differential Scanning Calorimetry (DSC)

- the effects of nanometric nickel (n-Ni) catalyst on the dehydrogenation and rehydrogenation behavior of ball milled lithium alanate (LiAlH<sub>4</sub>) 928
- Diffusion discussing the precipitation behavior of  $\boldsymbol{\sigma}$  phase using diffusion equation
- and thermodynamic simulation in dissimilar stainless steels 820 Diffusion barrier
- microstructural characteristics and degradation mechanism of the NiCrAlY/CrN/DSM11 system during thermal exposure at 1100 °C 77 Direct methanol fuel cells
- sol-gel synthesis of Pt-Ru-Os-Ir based anode electro-catalysts for direct methanol fuel cells 698

Directional solidification

- the microstructure parameters and microhardness of directionally solidified Ti-43Al-3Si alloy 593
- Doped BiFeO<sub>3</sub>
  - multiferroic properties and converse magnetoelectric effect in Bi<sub>1-x</sub>Ca<sub>x</sub>FeO<sub>3</sub> ceramics 537
- Double Gaussian distribution
  - measurement and modelling of the characteristic parameters for silver Schottky contacts on layered *p*-GaSe compound in a wide temperature range 51

Drop calorimetry

- calorimetric investigations on cubic  ${\rm BaTiO_3}$  and  ${\rm Ba}_{0.9}{\rm Nd}_{0.1}{\rm TiO_3}$  systems 565 DSC
  - surface oxidation and magnetic properties of  $({\rm Cu}_{60}{\rm Co}_{40})_{68}{\rm Zr}_{32}$  glassy ribbons 520

Dynamic permeability

ultra-high ferromagnetic resonance frequency in exchange-biased system 504

## EDX

surface oxidation and magnetic properties of  $(Cu_{60}Co_{40})_{68}Zr_{32}$  glassy ribbons 520

Egg-white

synthesis characterization and magnetic properties of Cr-substituted NiCuZn nanocrystalline ferrite 205

Egyptian kaolin

preparation, characterization and utilization of (Ni:Cu) bimetallic system loaded on zeolites 923

EIS

phase evolution and PEC performance of  $Zn_xCd_{(1-x)}S$  nanocrystalline thin films deposited by CBD 120

Elastic properties thermal energy of ionic solids 14 prediction study of the axial compressibility, anisotropy and dynamic properties for single crystal Ti<sub>2</sub>GeC 22 Electric properties effects of MnO doping on properties of 0.97K<sub>0.5</sub>Na<sub>0.5</sub>NbO<sub>3</sub>-0.03(Bi<sub>0.5</sub>K<sub>0.5</sub>)TiO<sub>3</sub> piezoelectric ceramics 323 Electrical conductivity stability and electrical property of  $Ba_{1-x}Sr_xCe_{0.8}Y_{0.2}O_{3-\delta}$  high temperature proton conductor 263 electrical conductivity and oxygen sensing behavior of  $SrSn_{1-x}Fe_xO_{3-\delta}$  (x = 0-0.2) 285 semiconducting properties of Ge-doped BaSnO<sub>3</sub> ceramic 678 structural, morphological and optical properties of nanocrystalline cadmium selenide thin films 849 influence of MoO<sub>2</sub> doping on structure and electrical conductivity of defect fluorite-type Gd<sub>2</sub>Zr<sub>2</sub>O<sub>7</sub> 868 Electro-catalyst sol-gel synthesis of Pt-Ru-Os-Ir based anode electro-catalysts for direct methanol fuel cells 698 Electrochemical hydrogen storage enhanced electrochemical characteristics of as-spun nanocrystalline and amorphous Mg<sub>2</sub>Ni-type alloy electrodes 749 Electrochemical impedance spectroscopy preparation and characterization of Li<sub>5</sub>ReSi<sub>4</sub>O<sub>12</sub> (Re = Nd, Gd) solid electrolyte 811 Electrochemical kinetic electrochemical characteristics of AB5-type hydrogen storage alloys 559 Electrochemical properties influence factors on electrochemical properties of Li<sub>4</sub>Ti<sub>5</sub>O<sub>12</sub>/C anode material pyrolyzed from lithium polyacrylate 160 synthesis and electrochemical properties of pure phase Zn<sub>2</sub>SnO<sub>4</sub> and composite Zn<sub>2</sub>SnO<sub>4</sub>/C 683 Electrochemical reactions comparisons of metallic clusters imbedded in the surface oxide of AB<sub>2</sub>, AB<sub>5</sub>, and A<sub>2</sub>B<sub>7</sub> alloys 831 the correlation of C14/C15 phase abundance and electrochemical properties in the AB<sub>2</sub> alloys 841 Electroless nickel-immersion gold (ENIG) effects of third element and surface finish on interfacial reactions of Sn-AgxCu (or Ni)/(Cu or ENIG) solder joints 331 Electrolyte influence of MoO<sub>3</sub> doping on structure and electrical conductivity of defect fluorite-type Gd<sub>2</sub>Zr<sub>2</sub>O<sub>7</sub> 868 preparation and characterization of proton conducting phosphosilicate glass membranes with different catalyst layers for low-temperature H<sub>2</sub>/O<sub>2</sub> fuel cells 902 Electromagnetic wave absorption enhanced absorption bandwidth in carbon-coated supermalloy FeNiMo nanocapsules for a thin absorb thickness 826 Electromechanical coupling coefficient  $(k_n)$ dielectric and piezoelectric characteristics of the non-stoichiometric (Na,K)NbO<sub>2</sub> ceramics doped with CuO 872 Electron microscopy compressibility and sinterability of Al2O3-YAG nanocomposite powder synthesized by an aqueous sol-gel method 640 Electronic band structure the electronic and magnetic properties of Sr<sub>2</sub>MnNbO<sub>6</sub>, Sr<sub>2</sub>FeMoO<sub>6</sub> and Sr<sub>2</sub>NiRuO<sub>6</sub> double perovskites: An LSDA + U + SOC study 456 Electronic structure first-principles study of elastic and electronic properties of MgZn<sub>2</sub> and ScZn<sub>2</sub> phases in Mg-Sc-Zn alloy 412 Electronic structures

first-principles study of elastic and electronic properties of MgZn<sub>2</sub> and ScZn<sub>2</sub>

electronic properties and europium ion photoluminescence behaviors in  $Sr_2CeO_4$  phosphor 950

980 Subject Index	κ of V
Electrospinning effect of Al doping on the visible photoluminescence of ZnO nanofibers 772	]
Energy absorption characteristic deformation and energy absorption characteristic of Al <sub>2</sub> O <sub>3f</sub> /Zn–Al composite foams during compression 620	]
Energy transfer	
a facile one-pot hydrothermal method to prepare europium-doped titania hollow phosphors and their sensitized luminescence properties 728	]
electronic properties and europium ion photoluminescence behaviors in Sr <sub>2</sub> CeO <sub>4</sub> phosphor 950 Energy transition	]
calculation on the energy transition coefficient by up-conversion emission intensity ratio 33	l
Epilayer's growth temperature	
effect of epilayer's growth temperature on crystalline quality of InAs <sub>0,6</sub> P <sub>0,4</sub> /InP grown by two-step growth method 530 Epitaxial growth	I
epitaxial growth of La <sub>0.7</sub> Sr <sub>0.3</sub> CoO <sub>3</sub> thin films on SrTiO <sub>3</sub> substrates by metal–	
organic deposition 483 Er <sup>3+</sup> /Yb <sup>3+</sup> co-doped	I
calculation on the energy transition coefficient by up-conversion emission intensity ratio 33	1
ESR	
preparation, characterization and utilization of (Ni:Cu) bimetallic system loaded on zeolites 923	]
Eu-doped thermal stable La <sub>2</sub> Ti <sub>2</sub> O <sub>7</sub> :Eu <sup>3+</sup> phosphors for blue-chip white LEDs with high color rendering index 338	I
Europium oxide	
template-free synthesis, characterization, growth mechanism and photoluminescence property of Eu(OH) <sub>3</sub> and Eu <sub>2</sub> O <sub>3</sub> nanospindles 446 Europium-doped	]
a facile one-pot hydrothermal method to prepare europium-doped titania hollow phosphors and their sensitized luminescence properties 728	l
Exchange bias ultra-high ferromagnetic resonance frequency in exchange-biased system 504	1
Exchange current density	
electrochemical characteristics of AB <sub>5</sub> -type hydrogen storage alloys 559	
Extrusion	
structure and consolidation of rapidly solidified Meso 10 alloy flakes 179 microstructural evolution during the annealing of an extruded AZ31 magnesium alloy 364	]
effect of extrusion temperature on microstructures and damping capacities of Grp/AZ91 composite 688	(
Fe	
a novel preparation of highly active iron-doped titania photocatalysts with a p-n junction semiconductor structure 877	(
FeAl intermetallic compound	
structural evolutions of the Fe–40Al–5Cr powders during mechanical alloying and subsequent heat treatment 963	(
Fe <sub>3</sub> O <sub>4</sub> nanoparticles	

magnetic properties and microwave absorption properties of carbon fibers coated by Fe<sub>3</sub>O<sub>4</sub> nanoparticles 93

#### Ferrite

structural and magnetic properties of  $Cu_xMg_{0.5-x}Zn_{0.5}Fe_2O_4$  (x = 0-0.5) particles 279

#### Ferroelectricity

ferroelectricity in the glassy material of the composition Bi<sub>2</sub>O<sub>3</sub>-Pb<sub>3</sub>O<sub>4</sub>-CuO-K<sub>2</sub>O 141

#### Ferroelectrics

- anisotropic properties and crystal structure of ferroelectric Na0.5Bi4.5Ti4O15 70
- phase-transition behavior and piezoelectric properties of lead-free  $(Ba_{0.95}Ca_{0.05})(Ti_{1-x}Zr_x)O_3$  ceramics 131
- the magneto-dielectric properties of compounds and alloys in the systems of TlInS<sub>2</sub>-TlFeS<sub>2</sub>, TlInS<sub>2</sub>-TlFeSe<sub>2</sub> 800

Ferromagnetic shape memory alloy

studies on ferromagnetic shape memory Ni-Mn-Ga alloys with Fe and rareearths additives 73

#### FESEM

study of electrical properties of nickel doped SnO<sub>2</sub> ceramic nanoparticles 237

#### Fill factor

n-Type polycrystalline (CdZn)Se photoelectrode synthesis and its photoelectrochemical characterizations 673

## Finite difference

characterization and thermal modelling of friction welded alumina-mild steel with the use of Al 1100 interlayer 703

#### First-principles calculations

first-principles study of elastic and electronic properties of MgZn<sub>2</sub> and ScZn<sub>2</sub> phases in Mg-Sc-Zn alloy 412

#### FLUOREX

controls of chromium and third element contents in nickel-base alloys for corrosion resistant alloys in hot HNO3-HF mixtures 194

#### Foams

isopropanol as an air-liquid interface reformer in the processing of cellular silica 308

## Formation energy

intrinsic vacancies in cubic-zirconia bulk and surface 898

#### Freeze casting

pore structure and mechanical properties in freeze cast porous Si<sub>3</sub>N<sub>4</sub> composites using polyacrylamide as an addition agent 423

## Friction

structural, mechanical and tribological properties of A356 aluminium alloy reinforced with Al<sub>2</sub>O<sub>3</sub>, SiC and SiC + graphite particles 631

## Friction welding

characterization and thermal modelling of friction welded alumina-mild steel with the use of Al 1100 interlayer 703

friction welding of titanium-tungsten pseudoalloy joints 761

## FT-IR

synthesis characterization and magnetic properties of Cr-substituted NiCuZn nanocrystalline ferrite 205

FTO-coated glass

a comparative study on structural, optical, photoconductivity properties of In and Al doped ZnO thin films grown onto glass and FTO substrates grown by spray pyrolysis process 548

Fused zirconia

preparation of partially stabilized zirconia from fused zirconia using roasting L5

## GaAs

- analysis of barrier height inhomogeneity in Au/n-GaAs Schottky barrier diodes by Tung model 418
- Gallium doped cadmium oxide

## temperature dependent structural, luminescent and XPS studies of CdO:Ga thin films deposited by spray pyrolysis 794

## GaN

investigations on the nonidealities in Pd/n-GaN Schottky diodes grown by MOCVD 615

## GaSe

measurement and modelling of the characteristic parameters for silver Schottky contacts on layered p-GaSe compound in a wide temperature range 51

## Gas-solid reactions

- effects of types of drying control chemical additives on the morphologies and electrochemical properties of Li<sub>4</sub>Ti<sub>5</sub>O<sub>12</sub> anode powders prepared by spray pyrolysis 913
- application of a new kinetic model for the hydriding kinetics of LaNi<sub>5-x</sub>Al<sub>x</sub>  $(0 \le x \le 1.0)$  alloys 63

Gaussian distribution

- analysis of the electrical characteristics of Zn/ZnSe/n-Si/Au-Sb structure fabricated using SILAR method as a function of temperature 388
- analysis of barrier height inhomogeneity in Au/n-GaAs Schottky barrier diodes by Tung model 418

HNO<sub>2</sub>-HF mixtures

 $Gd_2(Zr_{1-x}Mo_x)_2O_{7+2x}$ 

- influence of MoO<sub>3</sub> doping on structure and electrical conductivity of defect fluorite-type Gd<sub>2</sub>Zr<sub>2</sub>O<sub>7</sub> 868
- Glass forming range
  - calculation of glass forming ranges in Al–Ni–RE (Ce, La, Y) ternary alloys and their sub-binaries based on Miedema's model 377

Glass membrane

preparation and characterization of proton conducting phosphosilicate glass membranes with different catalyst layers for low-temperature H<sub>2</sub>/O<sub>2</sub> fuel cells 902

Glassy matrix

- study on Si–Ti alloy dispersed in a glassy matrix as an anode material for lithium-ion batteries 317
- Grain boundaries

effect of vanadium doping on the dielectric and nonlinear current–voltage characteristics of CaCu<sub>3</sub>Ti<sub>4</sub>O<sub>12</sub> ceramic 853

#### Grain growth

microstructural evolution during the annealing of an extruded AZ31 magnesium alloy 364

Grain refinement

- high-strength and high-conductive Cu/Ag multilayer produced by ARB 172 Graphene
- one-pot solvothermal syntheses and magnetic properties of graphene-based magnetic nanocomposites 136

Graphite particles

effect of extrusion temperature on microstructures and damping capacities of Grp/AZ91 composite 688

Green laser

light-induced coloration and transformation process in  $YAIO_3$  crystal 500

## $H_2/O_2$ fuel cell

preparation and characterization of proton conducting phosphosilicate glass membranes with different catalyst layers for low-temperature H<sub>2</sub>/O<sub>2</sub> fuel cells 902

Hall mobility

effects of annealing on cadmium selenide nanocrystalline thin films prepared by chemical bath deposition 892

Heat capacity

calorimetric investigations on cubic BaTiO<sub>3</sub> and Ba<sub>0.9</sub>Nd<sub>0.1</sub>TiO<sub>3</sub> systems 565 magnetic properties and magnetocaloric effect in Dy<sub>1-x</sub>Sc<sub>x</sub>Ni<sub>2</sub> solid solutions 626 microstructure, mechanical properties and wear behavior of metallic, nonmetallic and deep cryogenically chilled ASTM A216 WCB steel 645

Heat treatment

structure and electrical response of CaCu<sub>3</sub>Ti<sub>4</sub>O<sub>12</sub> ceramics: Effect of heat treatments at the high vacuum L1

#### HEMM

study on Si–Ti alloy dispersed in a glassy matrix as an anode material for lithium-ion batteries 317

Heterojunction semiconductor devices

electrical characterization of nanocluster n-CdO/p-Si heterojunction diode 188

- High entropy alloy
  - amorphization of equimolar alloys with HCP elements during mechanical alloying 210
- High pressure

microstructure evolution and precipitation of Al–12Mg alloy solidified under high pressure L12

High temperature

characterization of oxide scales to evaluate high temperature oxidation behavior of Ti(C,N)-based cermets in static air 461

High work function metal contacts

the growth of III–V nitrides heterostructure on Si substrate by plasmaassisted molecular beam epitaxy 343

High-frequency property

thickness dependence of magnetic properties in (Fe)<sub>0.73</sub>(Sm<sub>2</sub>O<sub>3</sub>)<sub>0.27</sub> nanogranular films 109

High-pressure annealing

magnetic and magnetostrictive properties in high-pressure synthesized  $Dy_{1-x}Pr_xFe_{1,9}(0 \le x \le 1)$  cubic Laves alloys 533

Ho:YAG ceramic fabrication, properties and laser performance of Ho:YAG transparent ceramic 745 Hot corrosion microstructural stability of zirconia-alumina composite coatings during hot corrosion test at 1050 °C 103 Hydrides mechanochemically driven nonequilibrium processes in MNH2-CaH2 systems (M = Li or Na) 224 Hydrogen absorbing materials application of a new kinetic model for the hydriding kinetics of  $LaNi_{5-v}Al_v(0)$  $\leq x \leq 1.0$ ) alloys 63 electrochemical characteristics of AB5-type hydrogen storage alloys 559 comparisons of metallic clusters imbedded in the surface oxide of AB<sub>2</sub>, AB<sub>5</sub>, and A<sub>2</sub>B<sub>7</sub> allovs 831 the correlation of C14/C15 phase abundance and electrochemical properties in the AB<sub>2</sub> alloys 841 Hydrogen insertion electrochemical characteristics of AB5-type hydrogen storage alloys 559 Hydrogen storage mechanochemically driven nonequilibrium processes in MNH2-CaH2 systems (M = Li or Na) 224 structural and thermal gas desorption properties of metal aluminum amides 297 Hydrogen storage materials metal halide doped metal borohydrides for hydrogen storage: The case of  $Ca(BH_{4})_{2}-CaX_{2}$  (X = F, Cl) mixture 721 the effects of nanometric nickel (n-Ni) catalyst on the dehydrogenation and rehydrogenation behavior of ball milled lithium alanate (LiAlH<sub>4</sub>) 928 Hydrogenation reaction

controls of chromium and third element contents in nickel-base alloys for

corrosion resistant alloys in hot HNO<sub>3</sub>-HF mixtures 194

preparation, characterization and utilization of (Ni:Cu) bimetallic system loaded on zeolites 923

Hydrothermal method

study on Raman spectra of zinc selenide nanopowders synthesized by hydrothermal method 327

#### Ilmenite

a novel process for producing synthetic rutile and LiFePO<sub>4</sub> cathode material from ilmenite 271

Immobilized titania nanoparticle

- immobilized titania nanophotocatalysis: Degradation, modeling and toxicity reduction of agricultural pollutants 155
- Impedance spectroscopy
  - influence of MoO<sub>3</sub> doping on structure and electrical conductivity of defect fluorite-type Gd<sub>2</sub>Zr<sub>2</sub>O<sub>7</sub> 868

InAs<sub>0.6</sub>P<sub>0.4</sub>

effect of epilayer's growth temperature on crystalline quality of  $InAs_{0.6}P_{0.4}/InP$  grown by two-step growth method 530

Influence factors

influence factors on electrochemical properties of  $Li_4Ti_5O_{12}/C$  anode material pyrolyzed from lithium polyacrylate 160

Infrared spectroscopy

synthesis and characterization of nano-crystalline  $Ce_{1-x}Gd_xO_{2-x/2}$  (x = 0-0.30) solid solutions 739

InGaN

the growth of III–V nitrides heterostructure on Si substrate by plasmaassisted molecular beam epitaxy 343

Inorganic compounds

- thermal energy of ionic solids 14
- Inorganic materials
  - a novel preparation of highly active iron-doped titania photocatalysts with a p-n junction semiconductor structure 877

effects of annealing on cadmium selenide nanocrystalline thin films prepared by chemical bath deposition 892

Interdiffusion

microstructural characteristics and degradation mechanism of the NiCrAlY/CrN/DSM11 system during thermal exposure at 1100 °C 77

Interface	Le
size dependence of creep behavior in nanoscale Cu/Co multilayer thin film 434	S
characterization and thermal modelling of friction welded alumina-mile steel with the use of Al 1100 interlayer 703	d Le
Interfacial reaction	Į.,
effects of third element and surface finish on interfacial reactions of Sn–Ag xCu (or Ni)/(Cu or ENIG) solder joints 331	– Le
Intermetallic compound (IMC) effects of third element and surface finish on interfacial reactions of Sn–Ag	– Le
xCu (or Ni)/(Cu or ENIG) solder joints 331	Le
Intermetallics	
microstructure development during directional solidification of Ti–45Al- 8Nb alloy 115	– Le
the microstructure parameters and microhardness of directionally solidified Ti-43Al-3Si alloy 593	d Lil
characterization and thermal modelling of friction welded alumina–mile steel with the use of Al 1100 interlayer 703	b
discussing the precipitation behavior of $\sigma$ phase using diffusion equation and thermodynamic simulation in dissimilar stainless steels 820	n Li-
Intrinsic vacancy intrinsic vacancies in cubic-zirconia bulk and surface 898	
Iron	
time-resolved photoluminescence study of stabilised iron-porous silicon nanocomposites 496	n Li[
Iron phosphate	
structural study and properties of a new iron phosphate Rb <sub>9</sub> Fe <sub>7</sub> (PO <sub>4</sub> ) <sub>10</sub> 56	9 Lil
Irradiation light-induced coloration and transformation process in YAIO <sub>3</sub> crystal 500	
Isopropanol	Li
isopropanol as an air-liquid interface reformer in the processing of cellula silica 308	
I-V characteristics	Lit
study of the <i>I</i> – <i>V</i> characteristics of SnO <sub>2</sub> :F/AgInS <sub>2</sub> (p)/Al Schottky diodes 49:	2
I–V measurements analysis of barrier height inhomogeneity in Au/n-GaAs Schottky barrie diodes by Tung model 418	er Lit
Kinetics	0
application of a new kinetic model for the hydriding kinetics of $\text{LaNi}_{5-x}\text{Al}_x$ ( $x \le x \le 1.0$ ) alloys 63	J
mechanically activated synthesis of single crystalline MgO nanostructure 715	S
glass-crystal transformations in $Se_{80-x}Te_{20}Ag_x$ (x = 0, 3, 5, 7 and 9) glasse 956	s Lit
Lanthanide alloys and compounds	Lit
magnetic properties of TbFe <sub>6</sub> Sn <sub>6</sub> from neutron diffraction and <sup>119</sup> Sr Mössbauer spectroscopy 36	
Laser performance	Li
fabrication, properties and laser performance of Ho:YAG transparent cerami 745	с
Laser remelting laser remelting of plasma-sprayed conventional and nanostructured Al <sub>2</sub> O <sub>3</sub> :	_ Lu
13 wt.%TiO <sub>2</sub> coatings on titanium alloy 356	
La <sub>2</sub> Ti <sub>2</sub> O <sub>7</sub>	
thermal stable La <sub>2</sub> Ti <sub>2</sub> O <sub>7</sub> :Eu <sup>3+</sup> phosphors for blue-chip white LEDs with hig color rendering index 338	h
$La_{(1-2x/3)}Sr_x(Mg_{0.5}Sn_{0.5})O_3$ substituting La <sup>3+</sup> with Sr <sup>2+</sup> to improve microwave dielectric properties of	f
La(Mg <sub>0.5</sub> Sn <sub>0.5</sub> )O <sub>3</sub> ceramics 441 Layered crystals	

Layered crystals

raman study of 2H-Mo<sub>1-x</sub> $W_xS_2$  layered mixed crystals 940

measurement and modelling of the characteristic parameters for silver Schottky contacts on layered *p*-GaSe compound in a wide temperature range 51

## Leaching

a novel process for producing synthetic rutile and LiFePO<sub>4</sub> cathode material from ilmenite 271

ead Magnesium Tungstate the phase evolution with temperature in 0.94PbZrO<sub>3</sub>-0.06Pb(Mg<sub>1/2</sub>W<sub>1/2</sub>)O<sub>3</sub> antiferroelectric ceramic 313

ead Zirconate

the phase evolution with temperature in 0.94PbZrO<sub>3</sub>-0.06Pb(Mg<sub>1/2</sub>W<sub>1/2</sub>)O<sub>3</sub> antiferroelectric ceramic 313

Lead-free ceramics

- crystal structure and properties of K<sub>0.5</sub>Na<sub>0.5</sub>NbO<sub>3</sub>–Bi<sub>0.5</sub>Na<sub>0.5</sub>TiO<sub>3</sub>–LiSbO<sub>3</sub> leadfree piezoelectric ceramics 407
- Lead-free piezoelectric ceramics

effects of MnO doping on properties of 0.97K<sub>0.5</sub>Na<sub>0.5</sub>NbO<sub>3</sub>-0.03(Bi<sub>0.5</sub>K<sub>0.5</sub>)TiO<sub>3</sub> piezoelectric ceramics 323

Leakage current

investigations on the nonidealities in Pd/n-GaN Schottky diodes grown by MOCVD 615

## .iFePO₄

- a novel process for producing synthetic rutile and LiFePO<sub>4</sub> cathode material from ilmenite 271
- Li-ion batteries
  - influence of Li addition on charge/discharge behavior of spinel lithium titanate 231
  - study on Si–Ti alloy dispersed in a glassy matrix as an anode material for lithium-ion batteries 317

Li[Li<sub>0.2</sub>Mn<sub>0.4</sub>Ni<sub>0.4</sub>]O<sub>2</sub>

spin-glass-like behavior in rhombohedral Li[Li<sub>(1/3-x/3</sub>)Mn<sub>(2/3-2x/3</sub>)Ni<sub>x</sub>]O<sub>2</sub> (x = 0.4) 488

LiNi<sub>0.65</sub>Co<sub>0.25</sub>Mn<sub>0.1</sub>O<sub>2</sub>

synthesis of  $\text{LiNi}_{0.65}\text{Co}_{0.25}\text{Mn}_{0.1}\text{O}_2$  as cathode material for lithium-ion batteries by rheological phase method 888

## Li2O doping

synthesis, characterization and physicochemical properties of nanosized Zn/Mn oxides system 541

Lithium alanate (LiAlH<sub>4</sub>)

the effects of nanometric nickel (n-Ni) catalyst on the dehydrogenation and rehydrogenation behavior of ball milled lithium alanate (LiAlH<sub>4</sub>) 928

Lithium ion batteries

- synthesis and electrochemical properties of pure phase  $Zn_2SnO_4$  and composite  $Zn_2SnO_4/C$  683
- synthesis and electrochemical properties of Li-rich spinel type  ${\rm LiMn_2O_4}$  powders by spray pyrolysis using aqueous solution of manganese carbonate 883
- synthesis of LiNi $_{0.65}$ Co $_{0.25}$ Mn $_{0.1}$ O $_2$  as cathode material for lithium-ion batteries by rheological phase method 888

## Lithium polyacrylate

influence factors on electrochemical properties of Li<sub>4</sub>Ti<sub>5</sub>O<sub>12</sub>/C anode material pyrolyzed from lithium polyacrylate 160

Lithium titanate

influence of Li addition on charge/discharge behavior of spinel lithium titanate 231

## Li<sub>4</sub>Ti<sub>5</sub>O<sub>12</sub>/C

influence factors on electrochemical properties of  ${\rm Li}_4{\rm Ti}_5{\rm O}_{12}/{\rm C}$  anode material pyrolyzed from lithium polyacrylate 160

## Luminescence

- tuning visible emission by choosing excitation wavelength in Mg-doped ZnO/silica composites 1
- structural and luminescent properties of YAG:Ce thin film phosphor 98 temperature dependence of morphology, structural and optical properties of
- ZnS nanostructures synthesized by wet chemical route 249 thermal stable  $La_2Ti_2O_7$ :Eu<sup>3+</sup> phosphors for blue-chip white LEDs with high color rendering index 338
- luminescence and absorbance of highly crystalline CaMoO<sub>4</sub>, SrMoO<sub>4</sub>, CaWO<sub>4</sub> and SrWO<sub>4</sub> nanoparticles synthesized by co-precipitation method at room temperature 475
- temperature dependent structural, luminescent and XPS studies of CdO:Ga thin films deposited by spray pyrolysis 794

#### Magentisation

magnetic properties and magnetocaloric effect in Dy<sub>1-x</sub>Sc<sub>x</sub>Ni<sub>2</sub> solid solutions 626

982

Magnesium alloy

- microstructural evolution during the annealing of an extruded AZ31 magnesium alloy 364
- Magnesium matrix composite
  - effect of extrusion temperature on microstructures and damping capacities of Grp/AZ91 composite 688
- Magnetic field
- electrochemical corrosion behavior in NaCl medium of zinc-nickel alloys electrodeposited under applied magnetic field 575 Magnetic hysteresis loops
- magnetic properties and microwave absorption properties of carbon fibers
  - coated by Fe<sub>3</sub>O<sub>4</sub> nanoparticles 93
- Magnetic materials
- multiferroic properties of BiFeO<sub>3</sub> doped Bi(MgTi)O<sub>3</sub>–PbTiO<sub>3</sub> ceramic system 815
- Magnetic measurements
- martensitic transition and magnetocaloric properties in Ni<sub>45</sub>Mn<sub>44-x</sub>Fe<sub>x</sub>Sn<sub>11</sub> alloys 516
- Magnetic oxides
  - the electronic and magnetic properties of  $Sr_2MnNbO_6$ ,  $Sr_2FeMoO_6$  and  $Sr_2NiRuO_6$  double perovskites: An LSDA + U + SOC study 456
- Magnetic phase diagram
  - effects of Fe substitution on structural and magnetic properties of the  $Nd_2Co_{7-x}Fe_x$  compounds 766
- Magnetic properties
  - studies on ferromagnetic shape memory Ni-Mn-Ga alloys with Fe and rareearths additives 73
  - one-pot solvothermal syntheses and magnetic properties of graphene-based magnetic nanocomposites 136
  - synthesis and characterization of nano-sized cobalt ferrite prepared via polyol method using conventional and microwave heating techniques 201
  - synthesis characterization and magnetic properties of Cr-substituted NiCuZn nanocrystalline ferrite 205
  - structural and magnetic properties of  $Cu_xMg_{0.5-x}Zn_{0.5}Fe_2O_4$  (x = 0–0.5) particles 279
  - size effect on the magnetic property of CoAl<sub>2</sub>O<sub>4</sub> nanopowders prepared by reverse micelle processing 395
  - magnetic and magnetostrictive properties in high-pressure synthesized  $Dy_{1-x}Pr_xFe_{1.9}(0 \le x \le 1)$  cubic Laves alloys 533
  - the magneto-dielectric properties of compounds and alloys in the systems of TlInS<sub>2</sub>-TlFeS<sub>2</sub>, TlInS<sub>2</sub>-TlFeSe<sub>2</sub> 800
- Magnetic susceptibility
- structural study and properties of a new iron phosphate  ${\rm Rb_9Fe_7(PO_4)_{10}}\,$  569 Magnetically ordered materials
  - magnetic properties and magnetocaloric effect in  $\mathrm{Dy}_{1-x}\mathrm{Sc}_x\mathrm{Ni}_2$  solid solutions 626
- Magnetism
- preparation and properties of (1 x)BiFeO<sub>3</sub>-xBaTiO<sub>3</sub> multiferroic ceramics 862 Magnetite
- one-pot solvothermal syntheses and magnetic properties of graphene-based magnetic nanocomposites 136
- Magnetocaloric
- magnetic properties and magnetocaloric effect in Dy<sub>1-x</sub>Sc<sub>x</sub>Ni<sub>2</sub> solid solutions 626
- Magnetocaloric effect
  - influence of irreversibility on inverse magnetocaloric and magnetoresistance properties of the  $\rm (Ni,Cu)_{50}Mn_{36}Sn_{14}$  alloys 508
  - martensitic transition and magnetocaloric properties in  $Ni_{45}Mn_{44-x}Fe_xSn_{11}$  alloys 516
- Magnetoresistance
- influence of irreversibility on inverse magnetocaloric and magnetoresistance properties of the (Ni,Cu)<sub>50</sub>Mn<sub>36</sub>Sn<sub>14</sub> alloys 508
- Magnetostriction
  - magnetic and magnetostrictive properties in high-pressure synthesized  $Dy_{1-x}Pr_xFe_{1,9}(0 \le x \le 1)$  cubic Laves alloys 533
- Magnetron sputtering
  - thermochromic property of La<sub>0.8</sub>Sr<sub>0.2</sub>MnO<sub>3</sub> thin-film material sputtered on quartz glass L22

- Manganese oxide
  - synthesis, characterization and physicochemical properties of nanosized Zn/Mn oxides system 541
- Martensite transformation
  - studies on ferromagnetic shape memory Ni–Mn–Ga alloys with Fe and rareearths additives 73
- Martensitic transition
  - influence of irreversibility on inverse magnetocaloric and magnetoresistance properties of the  $\rm (Ni,Cu)_{50}Mn_{36}Sn_{14}$  alloys 508
  - martensitic transition and magnetocaloric properties in  $\rm Ni_{45}Mn_{44-x}Fe_xSn_{11}$  alloys 516
- Materials science
- multiferroic properties of  $BiFeO_3$  doped  $Bi(MgTi)O_3$ -PbTiO<sub>3</sub> ceramic system 815 Mechanical alloying
  - microstructure and thermal stability of amorphous SiBCNAl powders fabricated by mechanical alloying 88
  - amorphization of equimolar alloys with HCP elements during mechanical alloying 210
  - synthesis of AlN–TiN nanostructured composite powder by reactive ball milling and subsequent thermal treatment 653
  - mechanically activated synthesis of single crystalline MgO nanostructures 715 structural evolutions of the Fe–40Al–5Cr powders during mechanical alloving and subsequent heat treatment 963
- Mechanical milling
  - mechanochemically driven nonequilibrium processes in  $MNH_2-CaH_2$  systems (M = Li or Na) 224
  - structural and thermal gas desorption properties of metal aluminum amides 297
- Mechanical properties
  - changes in short-range order of  $Zr_{55}Cu_{30}Al_{10}Ni_5$  and  $Zr_{55}Cu_{20}Al_{10}Ni_{10}Ti_5$  BMGs upon annealing ~85
  - laser remelting of plasma-sprayed conventional and nanostructured Al<sub>2</sub>O<sub>3</sub>-13 wt.%TiO<sub>2</sub> coatings on titanium alloy 356
  - first-principles study of elastic and electronic properties of  $\rm MgZn_2$  and  $\rm ScZn_2$  phases in Mg–Sc–Zn alloy  $\,$  412  $\,$
  - pore structure and mechanical properties in freeze cast porous Si<sub>3</sub>N<sub>4</sub> composites using polyacrylamide as an addition agent 423
  - effect of Y on microstructure and mechanical properties of duplex Mg-7Li alloys 468
  - structural and mechanical characterization of rapidly solidified  $Al_{95}Ni_5$  and  $Al_{93}Ni_5Mm_2$  alloys prepared by centrifugal atomization 581
  - mechanical property retention in remelted microparticle to nanoparticle  $AZ31/Al_2O_3$  composites 600
  - microstructure, mechanical properties and wear behavior of metallic, nonmetallic and deep cryogenically chilled ASTM A216 WCB steel 645 synthesis and mechanical properties of nano-layered composite 734
  - effect of rare-earth dopants on the growth and structural, optical, electrical and mechanical properties of L-arginine phosphate single crystals 784
- Mechanical quality factor  $(Q_m)$ dielectric and piezoelectric characteristics of the non-stoichiometric
  - (Na,K)NbO<sub>3</sub> ceramics doped with CuO 872
- Mechanoactivation
  - tailoring the microstructure of mechanoactivated  $\rm Al_2O_3$  and  $\rm SiO_2$  mixtures with TiO\_2 addition 777

Mechanochemical processing

- synthesis of AIN-TiN nanostructured composite powder by reactive ball milling and subsequent thermal treatment 653
- Melt spinning
  - enhanced electrochemical characteristics of as-spun nanocrystalline and amorphous Mg<sub>2</sub>Ni-type alloy electrodes 749
- Metal aluminum amide
  - structural and thermal gas desorption properties of metal aluminum amides 297
- Metal and alloys
  - sol–gel synthesis of Pt-Ru-Os-Ir based anode electro-catalysts for direct methanol fuel cells 698

Metal borohydrides

metal halide doped metal borohydrides for hydrogen storage: The case of  $Ca(BH_4)_2$ -CaX<sub>2</sub> (X = F, Cl) mixture 721

Metal hydride electrode

- comparisons of metallic clusters imbedded in the surface oxide of  $AB_2$ ,  $AB_5$ , and  $A_2B_7$  alloys 831
- the correlation of C14/C15 phase abundance and electrochemical properties in the AB<sub>2</sub> alloys 841

Metal hydrides

application of a new kinetic model for the hydriding kinetics of  $LaNi_{5-x}Al_x$  (0  $\leq x \leq 1.0$ ) alloys 63

Metal matrix composites

structural, mechanical and tribological properties of A356 aluminium alloy reinforced with Al<sub>2</sub>O<sub>3</sub>, SiC and SiC + graphite particles 631

Metallic glasses

surface oxidation and magnetic properties of  $(\mathrm{Cu}_{60}\mathrm{Co}_{40})_{68}\mathrm{Zr}_{32}$  glassy ribbons 520

Metallography

- microstructure, mechanical properties and wear behavior of metallic, nonmetallic and deep cryogenically chilled ASTM A216 WCB steel 645 discussing the precipitation behavior of σ phase using diffusion equation
- and thermodynamic simulation in dissimilar stainless steels 820 Metals and alloys
  - amorphization of equimolar alloys with HCP elements during mechanical alloying 210
  - structural and mechanical characterization of rapidly solidified Al<sub>95</sub>Ni<sub>5</sub> and Al<sub>93</sub>Ni<sub>5</sub>Mm<sub>2</sub> alloys prepared by centrifugal atomization 581

interactions of the components in the Al–V–Nd system at 773 K  $\,$  589 Metal-semiconductor  $\,$ 

catalyst-free combined synthesis of Zn/ZnO core/shell hollow microspheres and metallic Zn microparticles by thermal evaporation and condensation route 666

Metamagnetic transition

- antiferromagnetism of *Ln*RhO<sub>3</sub> (*Ln* = rare earth) 27
- Metastable
- phase transformation of metastable cubic  $\gamma$ -phase in U–Mo alloys 253 Methanol electrooxidation
- $RuO_2$ -SnO<sub>2</sub> nanocomposite electrodes for methanol electrooxidation 57 Mg-Li alloy
  - effect of Y on microstructure and mechanical properties of duplex Mg-7Li alloys 468

Mg<sub>2</sub>Ni-type alloy

- enhanced electrochemical characteristics of as-spun nanocrystalline and amorphous Mg<sub>2</sub>Ni-type alloy electrodes 749
- Mg-Sc-Zn alloy
  - first-principles study of elastic and electronic properties of MgZn<sub>2</sub> and ScZn<sub>2</sub> phases in Mg–Sc–Zn alloy 412

#### Microhardness

the microstructure parameters and microhardness of directionally solidified Ti-43Al-3Si alloy 593

Microstructure

- microstructure evolution and precipitation of Al–12Mg alloy solidified under high pressure L12
- microstructural characteristics and degradation mechanism of the NiCrAIY/CrN/DSM11 system during thermal exposure at 1100 °C 77
- microstructure and thermal stability of amorphous SiBCNAl powders fabricated by mechanical alloying 88
- microstructure development during directional solidification of Ti-45Al-8Nb alloy 115
- the influence of addition of Al nano-particles on the microstructure and shear strength of eutectic Sn–Ag–Cu solder on Au/Ni metallized Cu pads 216
- microstructural evolution during the annealing of an extruded AZ31 magnesium alloy 364
- pore structure and mechanical properties in freeze cast porous Si<sub>3</sub>N<sub>4</sub> composites using polyacrylamide as an addition agent 423
- structural and mechanical characterization of rapidly solidified Al<sub>95</sub>Ni<sub>5</sub> and Al<sub>93</sub>Ni<sub>5</sub>Mm<sub>2</sub> alloys prepared by centrifugal atomization 581
- structural, mechanical and tribological properties of A356 aluminium alloy reinforced with Al<sub>2</sub>O<sub>3</sub>, SiC and SiC + graphite particles 631
- microstructure, mechanical properties and wear behavior of metallic, nonmetallic and deep cryogenically chilled ASTM A216 WCB steel 645

- effect of extrusion temperature on microstructures and damping capacities of Grp/AZ91 composite 688
- synthesis and characterization of nano-crystalline  $Ce_{1-x}Gd_xO_{2-x/2}$  (x = 0–0.30) solid solutions 739
- fabrication, properties and laser performance of Ho:YAG transparent ceramic 745
- discussing the precipitation behavior of  $\sigma$  phase using diffusion equation and thermodynamic simulation in dissimilar stainless steels 820

## Microstructure evolution

laser remelting of plasma-sprayed conventional and nanostructured Al<sub>2</sub>O<sub>3</sub>-13 wt.%TiO<sub>2</sub> coatings on titanium alloy 356

#### Microwave

synthesis, characterization and properties of Ln(Ti<sub>0.8</sub>Sn<sub>0.2</sub>)TaO<sub>6</sub> (Ln = Nd, Sm) microwave ceramics 243

- Microwave absorber
  - a new microwave absorber based on antimony-doped tin oxide and ferrite composite with excellent electromagnetic match 347
- Microwave absorptive materials
- magnetic properties and microwave absorption properties of carbon fibers coated by  $Fe_3O_4$  nanoparticles 93
- Microwave technique
  - synthesis and characterization of nano-sized cobalt ferrite prepared via polyol method using conventional and microwave heating techniques 201
- Miedema's model
  - calculation of glass forming ranges in Al–Ni–RE (Ce, La, Y) ternary alloys and their sub-binaries based on Miedema's model 377

## Mn<sup>2+</sup>

- spectroscopic and crystal field studies of  $LiAIO_2:Mn^{2+}$  single crystals 4  $M_n$ +1AX<sub>n</sub>
- synthesis and mechanical properties of nano-layered composite 734 MnO doping
- effects of MnO doping on properties of 0.97K<sub>0.5</sub>Na<sub>0.5</sub>NbO<sub>3</sub>-0.03(Bi<sub>0.5</sub>K<sub>0.5</sub>)TiO<sub>3</sub> piezoelectric ceramics 323
- Mo content

controls of chromium and third element contents in nickel-base alloys for corrosion resistant alloys in hot HNO<sub>3</sub>–HF mixtures 194

#### MOCVD

- growth temperature effects on boron incorporation and optical properties of BGaAs/GaAs grown by MOCVD 10
- effect of epilayer's growth temperature on crystalline quality of  $InAs_{0.6}P_{0.4}/InP$  grown by two-step growth method 530

## MOD

epitaxial growth of La<sub>0.7</sub>Sr<sub>0.3</sub>CoO<sub>3</sub> thin films on SrTiO<sub>3</sub> substrates by metalorganic deposition 483

## Modeling

- immobilized titania nanophotocatalysis: Degradation, modeling and toxicity reduction of agricultural pollutants 155
- Monoclinic ZrO<sub>2</sub> phase
- preparation of partially stabilized zirconia from fused zirconia using roasting L5 Morphology
  - phase evolution and PEC performance of  $Zn_xCd_{(1-x)}S$  nanocrystalline thin films deposited by CBD 120

#### Mossbauer effect

- electrical conductivity and oxygen sensing behavior of  $SrSn_{1-x}Fe_xO_{3-\delta}$  (x = 0-0.2) 285
- Mössbauer spectroscopy
  - magnetic properties of  $\text{TbFe}_6\text{Sn}_6$  from neutron diffraction and  $^{119}\text{Sn}$  Mössbauer spectroscopy 36
- structural study and properties of a new iron phosphate  $\mathrm{Rb_9Fe_7(PO_4)_{10}}$  569 Mullite
- tailoring the microstructure of mechanoactivated  $\rm Al_2O_3$  and  $\rm SiO_2$  mixtures with TiO\_2 addition 777

Multiferroic

preparation and properties of (1 - x)BiFeO<sub>3</sub>-xBaTiO<sub>3</sub> multiferroic ceramics 862

## Multiferroic properties

multiferroic properties and converse magnetoelectric effect in Bi<sub>1-x</sub>Ca<sub>x</sub>FeO<sub>3</sub> ceramics 537

## Multilayer

high-strength and high-conductive Cu/Ag multilayer produced by ARB 172

## Na0.5Bi4.5Ti4O15

anisotropic properties and crystal structure of ferroelectric Na<sub>0.5</sub>Bi<sub>4.5</sub>Ti<sub>4</sub>O<sub>15</sub> 70

NaCl solution

electrochemical corrosion behavior in NaCl medium of zinc-nickel alloys electrodeposited under applied magnetic field 575

Nanocapsules

- enhanced absorption bandwidth in carbon-coated supermalloy FeNiMo nanocapsules for a thin absorb thickness 826
- Nanocomposite

RuO<sub>2</sub>-SnO<sub>2</sub> nanocomposite electrodes for methanol electrooxidation 57 one-pot solvothermal syntheses and magnetic properties of graphene-based magnetic nanocomposites 136

- Nanocrystalline
  - phase evolution and PEC performance of Zn<sub>x</sub>Cd<sub>(1-x</sub>)S nanocrystalline thin films deposited by CBD 120

Nano-doping

- the influence of addition of Al nano-particles on the microstructure and shear strength of eutectic Sn-Ag-Cu solder on Au/Ni metallized Cu pads 216
- Nano-granular film

thickness dependence of magnetic properties in (Fe)<sub>0.73</sub>(Sm<sub>2</sub>O<sub>3</sub>)<sub>0.27</sub> nanogranular films 109

- Nanoindentation
  - size dependence of creep behavior in nanoscale Cu/Co multilayer thin films 434

Nanomaterials

- electrical characterization of nanocluster n-CdO/p-Si heterojunction diode 188
- size effect on the magnetic property of  $CoAl_2O_4$  nanopowders prepared by reverse micelle processing 395

Nanometric nickel additive

the effects of nanometric nickel (n-Ni) catalyst on the dehydrogenation and rehydrogenation behavior of ball milled lithium alanate (LiAlH<sub>4</sub>) 928 Nanophotocatalysis

immobilized titania nanophotocatalysis: Degradation, modeling and toxicity reduction of agricultural pollutants 155

Nano-sized cobalt ferrite

- synthesis and characterization of nano-sized cobalt ferrite prepared via polyol method using conventional and microwave heating techniques 201
- Nanostructured composite
  - temperature dependence of morphology, structural and optical properties of ZnS nanostructures synthesized by wet chemical route 249
  - growth of novel ZnO nanostructures by soft chemical routes 351 the effects of calcination temperature on the electrochemical performance

of LiMnPO<sub>4</sub> prepared by ultrasonic spray pyrolysis 372

synthesis of AlN-TiN nanostructured composite powder by reactive ball milling and subsequent thermal treatment 653

Nanostructured materials

luminescence and absorbance of highly crystalline CaMoO<sub>4</sub>, SrMoO<sub>4</sub>, CaWO<sub>4</sub> and SrWO<sub>4</sub> nanoparticles synthesized by co-precipitation method at room temperature 475

- structural and mechanical characterization of rapidly solidified Al95Ni5 and Al<sub>93</sub>Ni<sub>5</sub>Mm<sub>2</sub> alloys prepared by centrifugal atomization 581
- sol-gel synthesis of Pt-Ru-Os-Ir based anode electro-catalysts for direct methanol fuel cells 698
- mechanically activated synthesis of single crystalline MgO nanostructures 715
- synthesis of zinc oxide nanoparticles elaborated by microemulsion method 944

## Nanostructures

- electrical characterization of nanocluster n-CdO/p-Si heterojunction diode 188
- template-free synthesis, characterization, growth mechanism and photoluminescence property of Eu(OH)<sub>3</sub> and Eu<sub>2</sub>O<sub>3</sub> nanospindles 446

Nano-TiN powder

microchemical and microstructural changes of nano-TiN powder during vacuum heat treatment 693

NaYF4

PEG-mediated solvothermal synthesis of NaYF<sub>4</sub>:Yb/Er superstructures with efficient upconversion luminescence L17

 $Nd_{2}Co_{7-x}Fe_{x}$ 

effects of Fe substitution on structural and magnetic properties of the  $Nd_2Co_{7-x}Fe_x$  compounds 766

Nd(Fe,Mo)<sub>12</sub>

nitrogenation effect of Nd(Fe,Mo)12 alloys prepared by strip casting technique 858

Negative photoconductivity

a comparative study on structural, optical, photoconductivity properties of In and Al doped ZnO thin films grown onto glass and FTO substrates grown by spray pyrolysis process 548

Neutron diffraction

magnetic properties of TbFe6Sn6 from neutron diffraction and 119Sn Mössbauer spectroscopy 36

Nickel tungsten allovs

- pulse co-electrodeposition and characterization of NiW-WC composite coatings 151
- Ni-Cr alloys

controls of chromium and third element contents in nickel-base alloys for corrosion resistant alloys in hot HNO<sub>3</sub>-HF mixtures 194

NiCuZn ferrite

synthesis characterization and magnetic properties of Cr-substituted NiCuZn nanocrystalline ferrite 205

- Nitrogenation
  - nitrogenation effect of Nd(Fe,Mo)12 alloys prepared by strip casting technique 858
- NKNS ceramics
  - dielectric and piezoelectric characteristics of the non-stoichiometric (Na,K)NbO<sub>3</sub> ceramics doped with CuO 872

Nonlinear optics

effect of rare-earth dopants on the growth and structural, optical, electrical and mechanical properties of L-arginine phosphate single crystals 784 Non-stoichiometric

- dielectric and piezoelectric characteristics of the non-stoichiometric (Na,K)NbO3 ceramics doped with CuO 872
- Non-uniform
  - microstructure evolution and precipitation of Al-12Mg alloy solidified under high pressure L12

## **Optical** materials

- tuning visible emission by choosing excitation wavelength in Mg-doped ZnO/silica composites 1
- temperature dependence of morphology, structural and optical properties of ZnS nanostructures synthesized by wet chemical route 249

spectral properties of Yb<sup>3+</sup> ions in Lu<sub>3</sub>ScAl<sub>4</sub>O<sub>12</sub> single crystal 513 Optical properties

- temperature-dependent study of the band-edge excitonic transitions of Cu<sub>2</sub>ZnSiS<sub>4</sub> single crystals by polarization-dependent piezoreflectance 46 spectral properties of Yb<sup>3+</sup> ions in Lu<sub>3</sub>ScAl<sub>4</sub>O<sub>12</sub> single crystal 513
- a comparative study on structural, optical, photoconductivity properties of In and Al doped ZnO thin films grown onto glass and FTO substrates grown by spray pyrolysis process 548
- catalyst-free combined synthesis of Zn/ZnO core/shell hollow microspheres and metallic Zn microparticles by thermal evaporation and condensation route 666
- semiconducting properties of Ge-doped BaSnO<sub>3</sub> ceramic 678
- fabrication, properties and laser performance of Ho:YAG transparent ceramic 745 effect of rare-earth dopants on the growth and structural, optical, electrical and mechanical properties of L-arginine phosphate single crystals 784
- physical properties of Ga-doped ZnO thin films by spray pyrolysis 788
- one-pot synthesis of Zn<sub>x</sub>Cd<sub>1-x</sub>S nanocrystals with tunable optical properties from molecular precursors 804
- effects of annealing on cadmium selenide nanocrystalline thin films prepared by chemical bath deposition 892

Optical spectroscopy

temperature-dependent study of the band-edge excitonic transitions of Cu<sub>2</sub>ZnSiS<sub>4</sub> single crystals by polarization-dependent piezoreflectance 46 luminescence and absorbance of highly crystalline CaMoO<sub>4</sub>, SrMoO<sub>4</sub>, CaWO<sub>4</sub> and SrWO<sub>4</sub> nanoparticles synthesized by co-precipitation method at room temperature 475

Ordering transformation

- structural evolutions of the Fe-40Al-5Cr powders during mechanical alloying and subsequent heat treatment 963 Oxidation
- surface oxidation and magnetic properties of (Cu<sub>60</sub>Co<sub>40</sub>)<sub>68</sub>Zr<sub>32</sub> glassy ribbons 520

Oxidation behavior

characterization of oxide scales to evaluate high temperature oxidation behavior of Ti(C,N)-based cermets in static air 461

Oxidation-resistance

- microstructural characteristics and degradation mechanism of the NiCrAIY/CrN/DSM11 system during thermal exposure at 1100 °C 77
- Oxide materials
  - enhanced thermoelectric properties of Nb-doped SrTiO<sub>3</sub> polycrystalline ceramic by titanate nanotube addition 293
- spectral properties of  $Yb^{3+}$  ions in  $Lu_3ScAl_4O_{12}$  single crystal 513 Oxide scales
  - characterization of oxide scales to evaluate high temperature oxidation behavior of Ti(C,N)-based cermets in static air 461

Oxides

- electrical characterization of nanocluster n-CdO/p-Si heterojunction diode 188
- electrical conductivity and oxygen sensing behavior of  $SrSn_{1-x}Fe_xO_{3-\delta}$  (x = 0-0.2) 285

## P25

a novel preparation of highly active iron-doped titania photocatalysts with a p-n junction semiconductor structure 877

Partially stabilized zirconia

preparation of partially stabilized zirconia from fused zirconia using roasting L5

PEC

phase evolution and PEC performance of  $Zn_xCd_{(1-x)}S$  nanocrystalline thin films deposited by CBD 120

Permanent magnets

a new microwave absorber based on antimony-doped tin oxide and ferrite composite with excellent electromagnetic match 347

Perovskites

multiferroic properties of BiFeO<sub>3</sub> doped Bi(MgTi)O<sub>3</sub>-PbTiO<sub>3</sub> ceramic system 815

semiconducting properties of Ge-doped  $BaSnO_3$  ceramic 678

Pervoskite

pervoskite-type  $BaCo_{0.7}Fe_{0.2}Ta_{0.1}O_{3-\delta}$  cathode for proton conducting IT-SOFC L8

Phase

- phase transformation of metastable cubic  $\gamma$ -phase in U–Mo alloys 253 Phase composition
- residual stress of  $Pb(Zr_xTi_{1-x})O_3$  films with mixed textures 167 Phase diagrams
  - interactions of the components in the Al–V–Nd system at 773 K 589 phase equilibria of the Zn–Bi–Ni system at 600 °C and 750 °C 125
- Phase evolution
  - amorphization of equimolar alloys with HCP elements during mechanical alloying 210
- Phase transition
  - anisotropic properties and crystal structure of ferroelectric Na<sub>0.5</sub>Bi<sub>4.5</sub>Ti<sub>4</sub>O<sub>15</sub> 70
  - glass-crystal transformations in  $Se_{80-x}Te_{20}Ag_x$  (x = 0, 3, 5, 7 and 9) glasses 956

Phase transitions

- microstructure development during directional solidification of Ti-45Al-8Nb alloy 115
- phase-transition behavior and piezoelectric properties of lead-free (Ba<sub>0.95</sub>Ca<sub>0.05</sub>)(Ti<sub>1-x</sub>Zr<sub>x</sub>)O<sub>3</sub> ceramics 131

discussing the precipitation behavior of  $\sigma$  phase using diffusion equation and thermodynamic simulation in dissimilar stainless steels 820

- effects of annealing on cadmium selenide nanocrystalline thin films prepared by chemical bath deposition 892
- Phosphate glass
  - calculation on the energy transition coefficient by up-conversion emission intensity ratio 33

## Phosphors

structural and luminescent properties of YAG:Ce thin film phosphor 98 thermal stable La<sub>2</sub>Ti<sub>2</sub>O<sub>2</sub>:Eu<sup>3+</sup> phosphors for blue-chip white LEDs with high

- color rendering index 338
- Photoelectrochemical cell
  - n-Type polycrystalline (CdZn)Se photoelectrode synthesis and its photoelectrochemical characterizations 673
- Photoluminescence
  - growth temperature effects on boron incorporation and optical properties of BGaAs/GaAs grown by MOCVD 10
  - synthesis, characterization and properties of Ln(Ti<sub>0.8</sub>Sn<sub>0.2</sub>)TaO<sub>6</sub> (Ln = Nd, Sm) microwave ceramics 243
  - template-free synthesis, characterization, growth mechanism and photoluminescence property of  $Eu(OH)_3$  and  $Eu_2O_3$  nanospindles 446
  - a facile one-pot hydrothermal method to prepare europium-doped titania hollow phosphors and their sensitized luminescence properties 728
  - effect of Al doping on the visible photoluminescence of ZnO nanofibers 772 physical properties of Ga-doped ZnO thin films by spray pyrolysis 788
  - electronic properties and europium ion photoluminescence behaviors in  $Sr_2CeO_4$  phosphor 950

Piezoelectric properties

- complete set of elastic, dielectric, and piezoelectric coefficients of [-1 0 1] poled  $0.23Pb(In_{1/2}Nb_{1/2}O_3)-0.45Pb(Mg_{1/3}Nb_{2/3})O_3-0.32PbTiO_3$  single crystals 428
- Piezoelectricity
  - phase-transition behavior and piezoelectric properties of lead-free  $(Ba_{0.05}Ca_{0.05})(Ti_{1-v}Zr_v)O_3$  ceramics 131
  - crystal structure and properties of K<sub>0.5</sub>Na<sub>0.5</sub>NbO<sub>3</sub>-Bi<sub>0.5</sub>Na<sub>0.5</sub>TiO<sub>3</sub>-LiSbO<sub>3</sub> leadfree piezoelectric ceramics 407

PIN-PMN-PT

- complete set of elastic, dielectric, and piezoelectric coefficients of [-1 0 1]
   poled 0.23Pb(In<sub>1/2</sub>Nb<sub>1/2</sub>O<sub>3</sub>)-0.45Pb(Mg<sub>1/3</sub>Nb<sub>2/3</sub>)O<sub>3</sub>-0.32PbTiO<sub>3</sub> single
   crystals 428
  PL
- the growth of III–V nitrides heterostructure on Si substrate by plasma-

assisted molecular beam epitaxy 343

- Plasma spray
  - microstructural stability of zirconia–alumina composite coatings during hot corrosion test at 1050 °C 103

Plasma spraying

laser remelting of plasma-sprayed conventional and nanostructured  $\rm Al_2O_3-13~wt.\%TiO_2$  coatings on titanium alloy ~356

p–n junction

a novel preparation of highly active iron-doped titania photocatalysts with a p–n junction semiconductor structure 877

Polyacrylamide

pore structure and mechanical properties in freeze cast porous  ${\rm Si_3N_4}$  composites using polyacrylamide as an addition agent 423

Polyol method

synthesis and characterization of nano-sized cobalt ferrite prepared via polyol method using conventional and microwave heating techniques 201

## Porosity

isopropanol as an air–liquid interface reformer in the processing of cellular silica 308

Porous silicon

time-resolved photoluminescence study of stabilised iron-porous silicon nanocomposites 496

Porous Si<sub>3</sub>N<sub>4</sub> ceramics

pore structure and mechanical properties in freeze cast porous Si<sub>3</sub>N<sub>4</sub> composites using polyacrylamide as an addition agent 423

## Powder metallurgy

structure and consolidation of rapidly solidified Meso 10 alloy flakes 179

Powders

synthesis and electrochemical properties of Li-rich spinel type  ${\rm LiMn_2O_4}$  powders by spray pyrolysis using aqueous solution of manganese carbonate 883

Precipitate phase

effect of Y on microstructure and mechanical properties of duplex Mg–7Li alloys 468

Precipitation

- microstructure evolution and precipitation of Al–12Mg alloy solidified under high pressure L12
- discussing the precipitation behavior of  $\sigma$  phase using diffusion equation and thermodynamic simulation in dissimilar stainless steels 820

Proton conductivity

preparation and characterization of proton conducting phosphosilicate glass membranes with different catalyst layers for low-temperature  $\rm H_2/O_2$  fuel cells 902

Proton conductor

stability and electrical property of  $Ba_{1-x}Sr_xCe_{0.8}Y_{0.2}O_{3-\delta}$  high temperature proton conductor 263

Pulse electroplating

pulse co-electrodeposition and characterization of NiW–WC composite coatings 151

Pyroelectricity

- ferroelectricity in the glassy material of the composition  $\rm Bi_2O_3-Pb_3O_4-CuO-K_2O~141$
- Quality factor
  - substituting La<sup>3+</sup> with Sr<sup>2+</sup> to improve microwave dielectric properties of La(Mg<sub>0.5</sub>Sn<sub>0.5</sub>)O<sub>3</sub> ceramics 441

Quasicrystals

- structure and consolidation of rapidly solidified Meso 10 alloy flakes 179 Quaternary
  - synthesis of CIGS powders: Transition from binary to quaternary crystalline structure 969

Quenching

- microstructure development during directional solidification of Ti-45Al-8Nb alloy 115
- Raman scattering
- raman study of 2H-Mo<sub>1-x</sub> $W_x$ S<sub>2</sub> layered mixed crystals 940

Raman spectroscopy

- study on Raman spectra of zinc selenide nanopowders synthesized by hydrothermal method 327
- synthesis and characterization of nano-crystalline  $Ce_{1-x}Gd_xO_{2-x/2}$  (x = 0–0.30) solid solutions 739

Rapid solidification

structure and consolidation of rapidly solidified Meso 10 alloy flakes 179 structural and mechanical characterization of rapidly solidified Al<sub>95</sub>Ni<sub>5</sub> and Al<sub>93</sub>Ni<sub>5</sub>Mm<sub>2</sub> alloys prepared by centrifugal atomization 581

Rare earth alloys and compounds

magnetic properties and magnetocaloric effect in Dy<sub>1-x</sub>Sc<sub>x</sub>Ni<sub>2</sub> solid solutions 626

Rare-earth compounds

magnetic and magnetostrictive properties in high-pressure synthesized  $Dy_{1-x}Pr_xFe_{1.9}(0 \le x \le 1)$  cubic Laves alloys 533

Rare-earth ion

antiferromagnetism of  $LnRhO_3$  (Ln = rare earth) 27

Rate capability

influence of Li addition on charge/discharge behavior of spinel lithium titanate 231

Rechargeable properties

synthesis and electrochemical properties of Li-rich spinel type LiMn<sub>2</sub>O<sub>4</sub> powders by spray pyrolysis using aqueous solution of manganese carbonate 883

Remaining glass

quantitative analysis of crystalline and remaining glass phases in CaO- $B_2O_3$ -SiO<sub>2</sub> ternary system glass ceramics 757

Remelting

mechanical property retention in remelted microparticle to nanoparticle  $AZ31/Al_2O_3$  composites 600

**Residual stress** residual stress of  $Pb(Zr_rTi_{1-r})O_3$  films with mixed textures 167 Resistivity comparative study of electrical properties of Cd and Te-enriched CdTe thin films at cryogenic temperature 661 the effect of Ti substitution for Cr on transport and thermoelectric properties of CrSb<sub>2</sub> at low temperatures 917 Rheological phase method synthesis of  $LiNi_{0.65}Co_{0.25}Mn_{0.1}O_2$  as cathode material for lithium-ion batteries by rheological phase method 888 Rhodium oxide antiferromagnetism of  $LnRhO_3$  (Ln = rare earth) 27 Rietveld method quantitative analysis of crystalline and remaining glass phases in CaO-B2O3-SiO<sub>2</sub> ternary system glass ceramics 757 RMS strain physical properties of Ga-doped ZnO thin films by spray pyrolysis 788 Roasting preparation of partially stabilized zirconia from fused zirconia using roasting L5 Rotatable anisotropy ultra-high ferromagnetic resonance frequency in exchange-biased system 504 Ruthenium-tin oxides RuO<sub>2</sub>-SnO<sub>2</sub> nanocomposite electrodes for methanol electrooxidation 57 SAD pattern analysis structure and consolidation of rapidly solidified Meso 10 alloy flakes 179 Sandwich structure analysis of the electrical characteristics of Zn/ZnSe/n-Si/Au-Sb structure fabricated using SILAR method as a function of temperature 388 Scanning electron microscope phase equilibria of the Zn-Bi-Ni system at 600 °C and 750 °C 125 Scanning electron microscopy magnetic properties and microwave absorption properties of carbon fibers coated by Fe<sub>3</sub>O<sub>4</sub> nanoparticles 93 the effects of calcination temperature on the electrochemical performance of LiMnPO<sub>4</sub> prepared by ultrasonic spray pyrolysis 372 study of obliquely deposited thin cobalt films 526 interactions of the components in the Al-V-Nd system at 773 K 589 mechanically activated synthesis of single crystalline MgO nanostructures 715 Schottky diode measurement and modelling of the characteristic parameters for silver Schottky contacts on layered *p*-GaSe compound in a wide temperature range 51 analysis of barrier height inhomogeneity in Au/n-GaAs Schottky barrier diodes by Tung model 418 investigations on the nonidealities in Pd/n-GaN Schottky diodes grown by MOCVD 615 Seeding materials the microstructure parameters and microhardness of directionally solidified Ti-43Al-3Si alloy 593 SEM high-strength and high-conductive Cu/Ag multilayer produced by ARB 172 the growth of III-V nitrides heterostructure on Si substrate by plasmaassisted molecular beam epitaxy 343 growth of novel ZnO nanostructures by soft chemical routes 351 surface oxidation and magnetic properties of  $(Cu_{60}Co_{40})_{68}Zr_{32}$  glassy ribbons 520 Semiconductors thermoelectric properties of the Cu<sub>2</sub>SnSe<sub>3</sub>-Cu<sub>2</sub>GeSe<sub>3</sub> solid solution 18 temperature-dependent study of the band-edge excitonic transitions of Cu<sub>2</sub>ZnSiS<sub>4</sub> single crystals by polarization-dependent piezoreflectance 46 temperature dependence of morphology, structural and optical properties of

ZnS nanostructures synthesized by wet chemical route 249 growth of novel ZnO nanostructures by soft chemical routes 351

- one-pot synthesis of  $Zn_xCd_{1-x}S$  nanocrystals with tunable optical properties from molecular precursors 804
- effects of annealing on cadmium selenide nanocrystalline thin films prepared by chemical bath deposition 892

synthesis of zinc oxide nanoparticles elaborated by microemulsion method 944

Shearing force

the influence of addition of Al nano-particles on the microstructure and shear strength of eutectic Sn–Ag–Cu solder on Au/Ni metallized Cu pads 216

Short fibers

deformation and energy absorption characteristic of Al<sub>2</sub>O<sub>3f</sub>/Zn–Al composite foams during compression 620

SHS/PHIP

- synthesis and mechanical properties of nano-layered composite 734 SILAR method
- analysis of the electrical characteristics of *Zn/ZnSe/n-Si/Au–Sb* structure fabricated using SILAR method as a function of temperature 388

Silica suspension

isopropanol as an air-liquid interface reformer in the processing of cellular silica 308

Silicon-based anode

study on Si–Ti alloy dispersed in a glassy matrix as an anode material for lithium-ion batteries 317

Silver iodide

- synthesis and characterization of AgI thin films at low temperature 268 Single crystals
  - complete set of elastic, dielectric, and piezoelectric coefficients of [-1 0 1] poled 0.23Pb(In<sub>1/2</sub>Nb<sub>1/2</sub>O<sub>3</sub>)-0.45Pb(Mg<sub>1/3</sub>Nb<sub>2/3</sub>)O<sub>3</sub>-0.32PbTiO<sub>3</sub> single crystals 428

Sintering

- phase-transition behavior and piezoelectric properties of lead-free  $(Ba_{0.05}Ca_{0.05})(Ti_{1-x}Zr_x)O_3$  ceramics 131
- compressibility and sinterability of Al<sub>2</sub>O<sub>3</sub>-YAG nanocomposite powder synthesized by an aqueous sol-gel method 640
- semiconducting properties of Ge-doped BaSnO<sub>3</sub> ceramic 678
- tailoring the microstructure of mechanoactivated  $\rm Al_2O_3$  and  $\rm SiO_2$  mixtures with TiO\_2 addition 777

Si–Ti alloys

study on Si–Ti alloy dispersed in a glassy matrix as an anode material for lithium-ion batteries 317

Sn-Ag-Cu solder

effects of third element and surface finish on interfacial reactions of Sn-AgxCu (or Ni)/(Cu or ENIG) solder joints 331

Sn-Ag-Ni solder

effects of third element and surface finish on interfacial reactions of Sn–Ag– xCu (or Ni)/(Cu or ENIG) solder joints 331

SOFC

pervoskite-type  $BaCo_{0.7}Fe_{0.2}Ta_{0.1}O_{3-\delta}$  cathode for proton conducting IT-SOFC L8

Sol-gel

- residual stress of  $Pb(Zr_xTi_{1-x})O_3$  films with mixed textures 167
- study of electrical properties of nickel doped  ${\rm SnO}_2$  ceramic nanoparticles 237
- development of cobalt ferrite powder preparation employing the sol-gel technique and its structural characterization 400
- the importance of the methanol content in the precursor solution, on the physical properties of cadmium oxide thin films prepared by the sol-gel method 554

Sol-gel process

sol–gel synthesis of Pt-Ru-Os-Ir based anode electro-catalysts for direct methanol fuel cells 698

Solid electrolyte

preparation and characterization of  $\text{Li}_5 \text{ReSi}_4 \text{O}_{12}$  (Re = Nd, Gd) solid electrolyte 811

Solid state hydrogen storage

- the effects of nanometric nickel (n-Ni) catalyst on the dehydrogenation and rehydrogenation behavior of ball milled lithium alanate (LiAlH<sub>4</sub>) 928 Solid-state reaction
  - influence factors on electrochemical properties of Li<sub>4</sub>Ti<sub>5</sub>O<sub>12</sub>/C anode material pyrolyzed from lithium polyacrylate 160

color rendering index 338
synthesis of AIN–TiN nanostructured composite powder by reactive ball
milling and subsequent thermal treatment 653
preparation and characterization of $Li_5ReSi_4O_{12}$ (Re = Nd, Gd) solid electrolyte
811
Solvothermal synthesis
PEG-mediated solvothermal synthesis of NaYF <sub>4</sub> :Yb/Er superstructures with
efficient upconversion luminescence L17
Spectral response
n-Type polycrystalline (CdZn)Se photoelectrode synthesis and its
photoelectrochemical characterizations 673
Spectroscopy
synthesis, characterization and properties of Ln(Ti <sub>0.8</sub> Sn <sub>0.2</sub> )TaO <sub>6</sub> (Ln = Nd, Sm)
microwave ceramics 243 Spinel structure
influence of Li addition on charge/discharge behavior of spinel lithium
titanate 231
development of cobalt ferrite powder preparation employing the sol-gel
technique and its structural characterization 400
Spin-glass-like
spin-glass-like behavior in rhombohedral Li[Li <sub>(1/3-x/3</sub> )Mn <sub>(2/3-2x/3</sub> )Ni <sub>x</sub> ]O <sub>2</sub>
(x = 0.4) 488
Spin–orbit effects
the electronic and magnetic properties of $Sr_2MnNbO_6$ , $Sr_2FeMoO_6$ and
$Sr_2NiRuO_6$ double perovskites: An LSDA + U + SOC study 456
Spin-reorientation
effects of Fe substitution on structural and magnetic properties of the
Nd <sub>2</sub> Co <sub>7-x</sub> Fe <sub>x</sub> compounds 766 Spontaneous pulverization
nitrogenation effect of Nd(Fe,Mo) <sub>12</sub> alloys prepared by strip casting
technique 858
Spray pyrolysis
physical properties of Ga-doped ZnO thin films by spray pyrolysis 788
synthesis and electrochemical properties of Li-rich spinel type LiMn <sub>2</sub> O <sub>4</sub>
powders by spray pyrolysis using aqueous solution of manganese
carbonate 883
Spray pyrolysis technique
study of the <i>I–V</i> characteristics of $SnO_2$ : F/AgInS <sub>2</sub> (p)/Al Schottky diodes 492
Sr <sub>2</sub> CeO <sub>4</sub> phosphor
electronic properties and europium ion photoluminescence behaviors in
Sr <sub>2</sub> CeO <sub>4</sub> phosphor 950
Stability pervoskite-type $BaCo_{0.7}Fe_{0.2}Ta_{0.1}O_{3-\delta}$ cathode for proton conducting IT-SOFC
L8
stability and electrical property of $Ba_{1-x}Sr_xCe_{0.8}Y_{0.2}O_{3-\delta}$ high temperature
proton conductor 263
State of charge
electrochemical characteristics of AB <sub>5</sub> -type hydrogen storage alloys 559
STEM
phase transformation and age-hardening of hexagonal $\alpha'$ martensite in Ti–
12 mass%V-2 mass%Al alloys studied by transmission electron
microscopy 607
Stress exponent size dependence of creep behavior in nanoscale Cu/Co multilayer thin films
Strip casting
nitrogenation effect of Nd(Fe,Mo) <sub>12</sub> alloys prepared by strip casting
technique 858
Stripe domains
thickness dependence of magnetic properties in (Fe) <sub>0.73</sub> (Sm <sub>2</sub> O <sub>3</sub> ) <sub>0.27</sub> nano-
granular films 109
Strontium cerate
stability and electrical property of $Ba_{1-x}Sr_xCe_{0.8}Y_{0.2}O_{3-\delta}$ high temperature
proton conductor 263
Strontium titanate
enhanced thermoelectric properties of Nb-doped SrTiO <sub>3</sub> polycrystalline

ceramic by titanate nanotube addition 293

thermal stable La Ti  $\Omega$  : Eu<sup>3+</sup> phosphore for blue, chip white IEDs with high

Structural evolution

- structural evolutions of the Fe–40Al–5Cr powders during mechanical alloying and subsequent heat treatment 963
- Structural properties
  - pulse co-electrodeposition and characterization of NiW-WC composite coatings 151

Substituting Ni with Mn

- enhanced electrochemical characteristics of as-spun nanocrystalline and amorphous  $Mg_2Ni$ -type alloy electrodes 749
- Superexchange interaction

antiferromagnetism of  $LnRhO_3$  (Ln = rare earth) 27

- Superstructures
  - PEG-mediated solvothermal synthesis of NaYF<sub>4</sub>:Yb/Er superstructures with efficient upconversion luminescence L17

## Support

- ${\rm RuO_2\text{-}SnO_2}$  nanocomposite electrodes for methanol electrooxidation 57 Surfactant
  - synthesis and electrochemical properties of Li-rich spinel type  ${\rm LiMn_2O_4}$  powders by spray pyrolysis using aqueous solution of manganese carbonate 883

Synthesis

one-pot solvothermal syntheses and magnetic properties of graphene-based magnetic nanocomposites 136

Synthetic rutile

a novel process for producing synthetic rutile and  ${\rm LiFePO}_4$  cathode material from ilmenite ~271

TEM

high-strength and high-conductive Cu/Ag multilayer produced by ARB 172 structure and consolidation of rapidly solidified Meso 10 alloy flakes 179 epitaxial growth of La<sub>0.7</sub>Sr<sub>0.3</sub>CoO<sub>3</sub> thin films on SrTiO<sub>3</sub> substrates by metalorganic deposition 483

- phase transformation and age-hardening of hexagonal α' martensite in Ti-12 mass%V-2 mass%Al alloys studied by transmission electron microscopy 607
- preparation, characterization and utilization of (Ni:Cu) bimetallic system loaded on zeolites 923

Temperature coefficient of resonant frequency

substituting La<sup>3+</sup> with Sr<sup>2+</sup> to improve microwave dielectric properties of La(Mg<sub>0.5</sub>Sn<sub>0.5</sub>)O<sub>3</sub> ceramics 441

Temperature dependent *I–V* measurement

- measurement and modelling of the characteristic parameters for silver Schottky contacts on layered *p*-GaSe compound in a wide temperature range 51
- Temperature profile

Texture

residual stress of  $Pb(Zr_xTi_{1-x})O_3$  films with mixed textures 167

microstructural evolution during the annealing of an extruded AZ31 magnesium alloy 364

- Thermal analysis
  - microstructure and thermal stability of amorphous SiBCNAl powders fabricated by mechanical alloying 88
  - crystallization kinetics of Mg<sub>61</sub>Cu<sub>28</sub>Gd<sub>11</sub> and (Mg<sub>61</sub>Cu<sub>28</sub>Gd<sub>11</sub>)<sub>99.5</sub>Sb<sub>0.5</sub> bulk metallic glasses 302

Thermal conductivity

the effect of Ti substitution for Cr on transport and thermoelectric properties of  ${\rm CrSb}_2$  at low temperatures 917

Thermal evaporation and condensation

catalyst-free combined synthesis of Zn/ZnO core/shell hollow microspheres and metallic Zn microparticles by thermal evaporation and condensation route 666

Thermal properties

thermal energy of ionic solids 14

Thermochromic

thermochromic property of  $\rm La_{0.8}Sr_{0.2}MnO_3$  thin-film material sputtered on quartz glass L22

Thermodynamic

calculation of glass forming ranges in Al–Ni–RE (Ce, La, Y) ternary alloys and their sub-binaries based on Miedema's model 377

Thermodynamic functions

calorimetric investigations on cubic  ${\rm BaTiO_3}$  and  ${\rm Ba}_{0.9}{\rm Nd}_{0.1}{\rm TiO_3}$  systems 565 Thermodynamic properties

prediction study of the axial compressibility, anisotropy and dynamic properties for single crystal Ti<sub>3</sub>GeC 22

metal halide doped metal borohydrides for hydrogen storage: The case of  $Ca(BH_4)_2$ -CaX<sub>2</sub> (X = F, Cl) mixture 721

Thermoelectric

thermoelectric properties of the Cu<sub>2</sub>SnSe<sub>3</sub>-Cu<sub>2</sub>GeSe<sub>3</sub> solid solution 18

enhanced thermoelectric properties of Nb-doped SrTiO<sub>3</sub> polycrystalline ceramic by titanate nanotube addition 293

#### Thermopower

the effect of Ti substitution for Cr on transport and thermoelectric properties of CrSb<sub>2</sub> at low temperatures 917

Thin cobalt films

study of obliquely deposited thin cobalt films 526

#### Thin films

- thermochromic property of La<sub>0.8</sub>Sr<sub>0.2</sub>MnO<sub>3</sub> thin-film material sputtered on quartz glass L22
- structural and luminescent properties of YAG:Ce thin film phosphor 98 synthesis and characterization of AgI thin films at low temperature 268 growth of novel ZnO nanostructures by soft chemical routes 351
- epitaxial growth of  $La_{0.7}Sr_{0.3}CoO_3$  thin films on  $SrTiO_3$  substrates by metal-organic deposition 483
- the importance of the methanol content in the precursor solution, on the physical properties of cadmium oxide thin films prepared by the sol-gel method 554
- comparative study of electrical properties of Cd and Te-enriched CdTe thin films at cryogenic temperature 661
- structural, morphological and optical properties of nanocrystalline cadmium selenide thin films 849

TiAl-based alloy

the microstructure parameters and microhardness of directionally solidified Ti-43Al-3Si alloy 593

## Ti<sub>3</sub>AlC<sub>2</sub>

synthesis and mechanical properties of nano-layered composite 734

Ti(C,N)-based cermets

characterization of oxide scales to evaluate high temperature oxidation behavior of Ti(C,N)-based cermets in static air 461

## Ti<sub>2</sub>GeC

prediction study of the axial compressibility, anisotropy and dynamic properties for single crystal Ti<sub>2</sub>GeC 22

- Time-resolved photoluminescence
  - time-resolved photoluminescence study of stabilised iron-porous silicon nanocomposites 496
- Tin oxide nanoparticles
- study of electrical properties of nickel doped  ${\rm SnO}_2$  ceramic nanoparticles ~237  ${\rm TiO}_2$ 
  - a novel preparation of highly active iron-doped titania photocatalysts with a p–n junction semiconductor structure 877
- Titania hollow spheres
  - a facile one-pot hydrothermal method to prepare europium-doped titania hollow phosphors and their sensitized luminescence properties 728

## Titanium

- friction welding of titanium-tungsten pseudoalloy joints 761 Titanium dioxide
  - tailoring the microstructure of mechanoactivated  $\rm Al_2O_3$  and  $\rm SiO_2$  mixtures with TiO\_2 addition 777
- Titanium-vanadium-aluminum alloy

phase transformation and age-hardening of hexagonal α' martensite in Ti-12 mass%V-2 mass%Al alloys studied by transmission electron microscopy 607

## Toop's model

calculation of glass forming ranges in Al–Ni–RE (Ce, La, Y) ternary alloys and their sub-binaries based on Miedema's model 377

characterization and thermal modelling of friction welded alumina-mild steel with the use of Al 1100 interlayer 703

Toxicity reduction

immobilized titania nanophotocatalysis: Degradation, modeling and toxicity reduction of agricultural pollutants 155

Transition layers

characterization of oxide scales to evaluate high temperature oxidation behavior of Ti(C,N)-based cermets in static air 461

Transition metal alloys

- comparisons of metallic clusters imbedded in the surface oxide of  $AB_2$ ,  $AB_5$ , and  $A_2B_7$  alloys 831
- the correlation of C14/C15 phase abundance and electrochemical properties in the AB<sub>2</sub> alloys 841
- Transition metal alloys and compounds
  - martensitic transition and magnetocaloric properties in  $\rm Ni_{45}Mn_{44-x}Fe_xSn_{11}$  alloys 516
- Transmission electron microscopy
  - the effects of calcination temperature on the electrochemical performance of  $LiMnPO_4$  prepared by ultrasonic spray pyrolysis 372
  - study of obliquely deposited thin cobalt films 526
  - microchemical and microstructural changes of nano-TiN powder during vacuum heat treatment 693
  - mechanically activated synthesis of single crystalline MgO nanostructures 715
- Transparent conductive oxides
  - the importance of the methanol content in the precursor solution, on the physical properties of cadmium oxide thin films prepared by the sol–gel method 554

## Tungsten carbide

- pulse co-electrodeposition and characterization of NiW-WC composite coatings 151
- Tungsten pseudoalloy D18
  - friction welding of titanium-tungsten pseudoalloy joints 761

Two-step growth method

effect of epilayer's growth temperature on crystalline quality of InAs<sub>0.6</sub>P<sub>0.4</sub>/InP grown by two-step growth method 530

## Uneven doping

a novel preparation of highly active iron-doped titania photocatalysts with a p-n junction semiconductor structure 877

Upconversion luminescence

PEG-mediated solvothermal synthesis of NaYF<sub>4</sub>:Yb/Er superstructures with efficient upconversion luminescence L17

#### Vacuum

structure and electrical response of CaCu<sub>3</sub>Ti<sub>4</sub>O<sub>12</sub> ceramics: Effect of heat treatments at the high vacuum L1

Vacuum heat treatment

microchemical and microstructural changes of nano-TiN powder during vacuum heat treatment 693

Variable emittance

thermochromic property of  $\rm La_{0.8}Sr_{0.2}MnO_3$  thin-film material sputtered on quartz glass L22

#### Wear

structural, mechanical and tribological properties of A356 aluminium alloy reinforced with Al<sub>2</sub>O<sub>3</sub>, SiC and SiC + graphite particles 631

Wet chemical method

magnetic properties and microwave absorption properties of carbon fibers coated by Fe<sub>3</sub>O<sub>4</sub> nanoparticles 93

#### Whisker

tailoring the microstructure of mechanoactivated Al<sub>2</sub>O<sub>3</sub> and SiO<sub>2</sub> mixtures with TiO<sub>2</sub> addition 777

Wolframite precursor method

the phase evolution with temperature in 0.94PbZrO<sub>3</sub>-0.06Pb(Mg<sub>1/2</sub>W<sub>1/2</sub>)O<sub>3</sub> antiferroelectric ceramic 313

#### XPS

surface oxidation and magnetic properties of  $(Cu_{60}Co_{40})_{68}Zr_{32}$  glassy ribbons 520

#### X-ray diffraction

phase-transition behavior and piezoelectric properties of lead-free (Ba<sub>0.95</sub>Ca<sub>0.05</sub>)(Ti<sub>1-v</sub>Zr<sub>v</sub>)O<sub>3</sub> ceramics 131

phase transformation of metastable cubic  $\gamma$ -phase in U–Mo alloys 253 growth of novel ZnO nanostructures by soft chemical routes 351

the effects of calcination temperature on the electrochemical performance of LiMnPO<sub>4</sub> prepared by ultrasonic spray pyrolysis 372

structural study and properties of a new iron phosphate  $Rb_9Fe_7(PO_4)_{10}~569$  interactions of the components in the Al–V–Nd system at 773 K ~589

effect of rare-earth dopants on the growth and structural, optical, electrical and mechanical properties of L-arginine phosphate single crystals 784

temperature dependent structural, luminescent and XPS studies of CdO:Ga thin films deposited by spray pyrolysis 794

glass-crystal transformations in Se $_{80-x}$ Te $_{20}$ Ag $_x$  (x = 0, 3, 5, 7 and 9) glasses 956 X-ray diffraction pattern

- substituting La<sup>3+</sup> with Sr<sup>2+</sup> to improve microwave dielectric properties of  $La(Mg_{0,5}Sn_{0,5})O_3$  ceramics 441
- X-ray diffraction (XRD)

the effects of nanometric nickel (n-Ni) catalyst on the dehydrogenation and rehydrogenation behavior of ball milled lithium alanate (LiAlH<sub>4</sub>) 928

X-ray photoelectron spectroscopy (XPS)

microchemical and microstructural changes of nano-TiN powder during vacuum heat treatment 693

X-ray photoemission spectroscopy

electrical conductivity and oxygen sensing behavior of  $SrSn_{1-x}Fe_xO_{3-\delta}$  (x = 0-0.2) 285

#### X-ray scattering

structural, morphological and optical properties of nanocrystalline cadmium selenide thin films 849

## X-ray techniques

quantitative analysis of crystalline and remaining glass phases in CaO–B<sub>2</sub>O<sub>3</sub>– SiO<sub>2</sub> ternary system glass ceramics 757

XRD

- study of electrical properties of nickel doped SnO<sub>2</sub> ceramic nanoparticles 237
- the growth of III-V nitrides heterostructure on Si substrate by plasmaassisted molecular beam epitaxy 343
- surface oxidation and magnetic properties of  $(Cu_{60}Co_{40})_{68}Zr_{32}$  glassy ribbons 520
- preparation, characterization and utilization of (Ni:Cu) bimetallic system loaded on zeolites 923

## YAG:Ce

- structural and luminescent properties of YAG:Ce thin film phosphor 98 YAIO<sub>2</sub> crystal
- light-induced coloration and transformation process in  $\mathrm{YAIO}_3$  crystal 500 Yttrium
  - effect of Y on microstructure and mechanical properties of duplex Mg–7Li alloys 468

## Zeolites

- preparation, characterization and utilization of (Ni:Cu) bimetallic system loaded on zeolites 923
- Zinc manganite synthesis, characterization and physicochemical properties of nanosized Zn/Mn oxides system 541

## Zinc oxide

- synthesis, characterization and physicochemical properties of nanosized Zn/Mn oxides system 541
- a comparative study on structural, optical, photoconductivity properties of In and Al doped ZnO thin films grown onto glass and FTO substrates grown by spray pyrolysis process 548

Zinc selenide powder

study on Raman spectra of zinc selenide nanopowders synthesized by hydrothermal method 327

Zirconia–Alumina composite

microstructural stability of zirconia–alumina composite coatings during hot corrosion test at 1050 °C 103 deformation and energy absorption characteristic of Al<sub>2</sub>O<sub>3f</sub>/Zn–Al composite foams during compression 620

Zn-based alloy

phase equilibria of the Zn–Bi–Ni system at 600  $^\circ C$  and 750  $^\circ C$  125 Zn–Bi–Ni system

phase equilibria of the Zn–Bi–Ni system at 600  $^\circ C$  and 750  $^\circ C~$  125 Zn–Ni alloy

electrochemical corrosion behavior in NaCl medium of zinc–nickel alloys electrodeposited under applied magnetic field 575

ZnO

physical properties of Ga-doped ZnO thin films by spray pyrolysis 788 ZnO nanofibers

effect of Al doping on the visible photoluminescence of ZnO nanofibers 772

## ZnSe

analysis of the electrical characteristics of *Zn/ZnSe/n-Si/Au–Sb* structure fabricated using SILAR method as a function of temperature 388

 $Zn_2SnO_4$ 

synthesis and electrochemical properties of pure phase  $Zn_2SnO_4$  and composite  $Zn_2SnO_4/C$  683

 $Zn_2SnO_4/C$ 

synthesis and electrochemical properties of pure phase Zn<sub>2</sub>SnO<sub>4</sub> and composite Zn<sub>2</sub>SnO<sub>4</sub>/C 683

 $Zn_xCd_{1-x}S$ 

one-pot synthesis of Zn<sub>x</sub>Cd<sub>1-x</sub>S nanocrystals with tunable optical properties from molecular precursors 804